

2020-11-23

Mitochondrial respiration contributes to the interferon gamma response in antigen presenting cells [preprint]

Michael C. Kiritsy
University of Massachusetts Medical School

Et al.

Let us know how access to this document benefits you.

Follow this and additional works at: https://escholarship.umassmed.edu/faculty_pubs



Part of the [Immunity Commons](#), [Immunology of Infectious Disease Commons](#), and the [Immunopathology Commons](#)

Repository Citation

Kiritsy MC, Mott D, Behar SM, Sasseti CM, Olive AJ. (2020). Mitochondrial respiration contributes to the interferon gamma response in antigen presenting cells [preprint]. University of Massachusetts Medical School Faculty Publications. <https://doi.org/10.1101/2020.11.22.393538>. Retrieved from https://escholarship.umassmed.edu/faculty_pubs/1840

Creative Commons License



This work is licensed under a [Creative Commons Attribution-NonCommercial 4.0 License](#). This material is brought to you by eScholarship@UMMS. It has been accepted for inclusion in University of Massachusetts Medical School Faculty Publications by an authorized administrator of eScholarship@UMMS. For more information, please contact Lisa.Palmer@umassmed.edu.

1 **Title: Mitochondrial respiration contributes to the interferon gamma response in antigen**
2 **presenting cells**

3
4 Short-title: Interferon gamma signaling requires complex I

5
6 Authors: Michael C. Kiritsy^a, Daniel Mott^a, Samuel M. Behar^a, Christopher M. Sasseti^{a#},
7 Andrew J. Olive^{b#}

8
9
10
11
12 ^aDepartment of Microbiology and Physiological Systems, University of Massachusetts Medical
13 School, 55 Lake Ave. N, Worcester, Massachusetts 01655, USA.

14
15 ^b Department of Microbiology & Molecular Genetics, Michigan State University, 567 Wilson
16 Road, East Lansing, MI, 48824, USA.

17
18 # Co-corresponding Author

19
20
21 Correspondence:

22
23 Christopher Sasseti
24 christopher.sasseti@umassmed.edu
25 Dept. of Microbiology and Physiological Systems
26 University of Massachusetts Medical School
27 368 Plantation St. ASC8-2051
28 Worcester, MA 01605
29 (508) 856-3678

30
31 Andrew Olive
32 oliveand@msu.edu
33 Department of Microbiology and Molecular Genetics
34 Michigan State University
35 567 Wilson Rd BPS5198
36 East Lansing, MI 48824
37 (517) 884-5367

38
39
40
41

42 **Abstract:**

43

44 The immunological synapse allows antigen presenting cells (APC) to convey a wide array of
45 functionally distinct signals to T cells, which ultimately shape the immune response. The relative
46 effect of stimulatory and inhibitory signals is influenced by the activation state of the APC,
47 which is determined by an interplay between signal transduction and metabolic pathways. While
48 toll-like receptor ligation relies on glycolytic metabolism for the proper expression of
49 inflammatory mediators, little is known about the metabolic dependencies of other critical
50 signals such as interferon gamma (IFN γ). Using CRISPR-Cas9, we performed a series of
51 genome-wide knockout screens in macrophages to identify the regulators of IFN γ -inducible T
52 cell stimulatory or inhibitory proteins MHCII, CD40, and PD-L1. Our multi-screen approach
53 enabled us to identify novel pathways that control these functionally distinct markers. Further
54 integration of these screening data implicated complex I of the mitochondrial respiratory chain in
55 the expression of all three markers, and by extension the IFN γ signaling pathway. We report that
56 the IFN γ response requires mitochondrial respiration, and APCs are unable to activate T cells
57 upon genetic or chemical inhibition of complex I. These findings suggest a dichotomous
58 metabolic dependency between IFN γ and toll-like receptor signaling, implicating mitochondrial
59 function as a fulcrum of innate immunity.

60

61

62

63

64

65 **Introduction:**

66 During the initiation of an adaptive immune response, the antigen presenting cell (APC) serves
67 as an integration point where tissue-derived signals are conveyed to T cells. Myeloid APCs, such
68 as macrophages and dendritic cells (DCs), are responsible for the display of specific peptides in
69 complex with MHC molecules, and for the expression of co-signaling factors that tune the T cell
70 response (1). The expression of stimulatory or inhibitory co-signaling molecules depends on the
71 local immune environment and activation state of the APC (2). In particular, interferon gamma
72 ($\text{IFN}\gamma$) stimulates the surface expression of MHC proteins (3-9), co-stimulatory proteins such as
73 CD40, and the secretion of cytokines like IL-12 and IL-18 (10), to promote T cell activation and
74 the production of $\text{IFN}\gamma$ -producing T-helper type 1 (Th1) effector cells (11-15). In the context of
75 local inflammation, pattern recognition receptor (PRR) ligands and endogenous immune
76 activators can collaborate with $\text{IFN}\gamma$ to induce the expression of co-inhibitory molecules, like
77 programmed death-ligand 1 (PD-L1) (16-22), which ligates T cell programmed death receptor 1
78 (PD1) to limit immune activation and mitigate T cell-mediated tissue damage (23-26).

79
80 $\text{IFN}\gamma$ mediates these complex effects via binding to a heterodimeric surface receptor (27-
81 30). The subunits of the complex, IFNGR1 and IFNGR2, assemble once IFNGR1 is bound by its
82 ligand (31, 32). Complex assembly promotes the phosphorylation of janus kinases 1 and 2 (JAK1
83 and JAK2) followed by activation of the signal transducer and activation of transcription 1
84 (STAT1) (33). Phosphorylated STAT1 then dimerizes and translocates to the nucleus to activate
85 the transcription of genes containing promoters with $\text{IFN}\gamma$ -activated sequences (GAS), which
86 includes other transcription factors such as interferon regulatory factor 1 (*Irf1*) that amplify the
87 expression of a large regulon that includes T cell co-signaling molecules (34, 35). The

88 importance of this signaling pathway is evident in a variety of diseases including cancer (36-40),
89 autoimmunity (41, 42), and infection (43). Individuals with inborn deficiencies in IFN γ
90 signaling, including mutations to the receptor (44, 45), suffer from a defect in Th1 immunity that
91 results in an immunodeficiency termed Mendelian susceptibility to mycobacterial disease
92 (MSMD) (46-49). Conversely, antagonists of IFN γ -inducible inhibitory molecules, such as PD-
93 L1, are the basis for checkpoint inhibitor therapies that effectively promote T cell-mediated
94 tumor destruction (26, 28, 50-55). While the obligate components of the IFN γ signaling pathway
95 are well known, characterization of additional regulators of this response promises to identify
96 both additional causes of immune dysfunction and new therapeutic targets.

97
98 Recent data suggests that cellular metabolism is an important modulator of the APC-T
99 cell interaction. In particular, microbial stimulation of PRR receptors on the APC induces
100 glycolytic metabolism and this shift in catabolic activity is essential for cellular activation,
101 migration, and CD4⁺ and CD8⁺ T cell activation (18, 56-70). The metabolic state of the T cell is
102 also influenced by the local environment and determines both effector function and long-term
103 differentiation into memory cells (71, 72). Like PRR signaling, IFN γ stimulation has been
104 reported to stimulate glycolysis and modulate cellular metabolism in macrophages (66, 73).
105 However, the effects of different metabolic states on IFN γ -stimulated APC function remains
106 unclear.

107
108 To globally understand the cellular pathways that influence IFN γ -dependent APC
109 function, we used a CRISPR-Cas9 knockout library (74) in macrophages to perform a series of
110 parallel forward-genetic screens for regulators of three IFN γ -inducible co-signaling molecules:

111 MHCII, CD40, and PD-L1. We identified positive and negative regulators that controlled each
112 marker, underscoring the complex regulatory networks that influence the interactions between
113 APCs and T cells. Pooled analysis of the screens uncovered shared regulators that contribute to
114 the global IFN γ response. Prominent among these general regulators was complex I of the
115 respiratory chain. We report that the activity of the IFN γ receptor complex and subsequent
116 transcriptional activation depends on mitochondrial function in both mouse and human myeloid
117 cells. Experimental perturbation of respiration inhibits the capacity of both macrophages and
118 dendritic cells to stimulate T cells, identifying mitochondrial function as a central point where
119 local signals are integrated to determine APC function.

120

121 **Results**

122

123 **Forward genetic screen identifies regulators of IFN γ -inducible MHCII, CD40 and PD-L1** 124 **cell surface expression.**

125

126 To investigate the diverse regulatory pathways underlying the IFN γ response, we
127 examined the expression of three functionally distinct cell surface markers that are induced by
128 IFN γ . Stimulation of Cas9-expressing immortalized bone marrow-derived macrophages with
129 IFN γ for 24 hours resulted in the upregulation of T cell stimulatory molecules, major
130 histocompatibility complex class II (MHCII) and CD40, and the inhibitory ligand PD-L1
131 (*Cd274*), on the cell surface (Figure 1A). To identify genes that regulate the expression of these
132 markers, Cas9-expressing macrophages were transduced with a lentiviral genome-wide knockout
133 (KO) library containing four single guide RNAs (sgRNAs) per protein-coding gene and 1000

134 non-targeting control (NTC) sgRNAs (74). The knockout library was then stimulated with IFN γ ,
135 and fluorescently activated cell sorting (FACS) was used to select for mutants with high or low
136 cell surface expression of each individual marker (Figure 1B). For each of the three surface
137 markers, positive and negative selections were performed in duplicate. The sgRNAs contained in
138 the input library and each sorted population were amplified and sequenced (Figure 1A,B).

139 To estimate the strength of selection on individual mutant cells, we specifically assessed
140 the relative abundance of cells harboring sgRNAs that target each of the surface markers that
141 were the basis for cell sorting. When the abundances of sgRNAs specific for *H2-Ab1* (encoding
142 the MHCII, H2-I-A beta chain), *Cd40*, or *Cd274* (PD-L1) were compared between high- and
143 low-expressing cell populations, we found that each of these sgRNAs were significantly depleted
144 from the cell populations expressing the targeted surface molecule, while each had no consistent
145 effect on the expression of non-targeted genes (Figure 1C). While not all individual sgRNAs
146 produced an identical effect, we found that targeting the genes that served as the basis of sorting
147 altered the mean relative abundance 30-60 fold, demonstrating that all selections efficiently
148 differentiated responsive from non-responsive cells.

149 We next tested for statistical enrichment of sgRNAs using MAGeCK-MLE (75), which
150 employs a generalized linear model to identify genes, and by extension regulatory mechanisms,
151 controlling the expression of each surface marker. This analysis correctly identified the
152 differential representation of sgRNAs targeting genes for the respective surface marker in the
153 sorted populations in each screen, which were found in the top 20 ranked negative selection
154 scores (Ranks: *H2-Ab1* = 20, *Cd40* = 1, *Cd274* = 3; Table S1). Upon unsupervised clustering of
155 β scores for the most highly enriched genes in each screen (top 5%, positive or negative) both
156 common and pathway-specific effects were apparent (Figure 1D; Table S2). A small number of

157 genes assigned to Cluster 1, including the IFN γ receptor components (*Ifngr1* and *Ifngr2*), were
158 strongly selected in the non-responsive population in all three selections. However, many
159 mutations appeared to preferentially affect the expression of individual surface markers,
160 including a number of known pathway-specific functions. For example, genes previously shown
161 to specifically control MHCII transcription, such as *Ciita*, *Rfx5*, *Rfxap*, *Rfxank*, and *Creb1* (8, 76-
162 78) were found in Cluster 4 along with several novel regulators that appear to be specifically
163 required for this pathway. MHCII-specific factors are reported in an accompanying study (79).

164 Genes specifically required for CD40 expression in Cluster 3 included the heterodimeric
165 receptor for TNF. *Tnfrsf1a* and *Tnfrsf1b* were the 6th and 50th lowest β scores in the CD40
166 screen, respectively. Previous studies suggested that TNF stimulation enhances IFN γ -mediated
167 CD40 expression in hematopoietic progenitors (80), and we confirmed this observation in
168 macrophages (Figure 1E). We observed a 6-fold higher induction of CD40 in macrophages
169 stimulated with a combination of IFN γ and TNF compared to IFN γ alone. This synergy was
170 specific to CD40 induction, as we did not observe any enhancement of IFN γ -induced MHCII
171 expression by TNF addition.

172 Several recent studies identified genes that control PD-L1 expression in cancer cell
173 lines(28, 53, 55, 81-86), and we validated the PD-L1-associated clusters using these candidates.
174 Our analysis found the previously-described negative regulators, *Irf2* (87), *Keap1*, and *Cul3* (88-
175 90) in the PD-L1-related Cluster 7, along with novel putative negative regulators such as the
176 oligosaccharyltransferase complex subunit *Ostc* and the transcriptional regulator, *Cnbp*. We
177 generated knockout macrophages for each of these novel candidates and confirmed that mutation
178 of these genes enhances the IFN γ -dependent induction of PD-L1 surface levels (Figure 1F).

179 Cumulatively, these data delineate the complex regulatory networks that shape the IFN γ
180 response.

181

182 **Mitochondrial complex I is a positive regulator of the IFN γ response.**

183 To identify global regulators of the IFN γ response, we performed a combined analysis,
184 reasoning that treating each independent selection as a replicate measurement would increase our
185 power to identify novel pathways. We used MAGeCK to calculate a selection coefficient (β) for
186 each gene by maximum likelihood estimation (75). By combining the 24 available measurements
187 for each gene (three different markers, each selection in duplicate, and four sgRNAs per gene),
188 we found that the resulting selection coefficient reflected the global importance of a gene for the
189 IFN γ response (Table S3). The most important positive regulators corresponded to the proximal
190 IFN γ signaling complex (Figure 2A). Similarly, we identified known negative regulators of IFN γ
191 signaling, including the protein inhibitor of activated Stat1 (*Pias1*) (91), protein tyrosine
192 phosphatase non-receptor type 2 (*Ptpn2*) (84), Mitogen activate protein kinase 1 (*Mapk1*), and
193 suppressor of cytokine signaling 1 (*Socs1*) and 3 (*Socs3*).

194 We performed gene set enrichment analysis (GSEA) using a ranked list of positive
195 regulators from the combined analysis (Table S4) (92). Among the top enriched pathways was a
196 gene set associated with type II interferon (e.g., IFN γ) signaling (normalized enrichment score =
197 2.45, q-value = 7.98e-5), validating the approach. GSEA identified a similarly robust enrichment
198 for gene sets related to mitochondrial respiration and oxidative phosphorylation (Figure 2B). In
199 particular, we found a significant enrichment of gene sets dedicated to the assembly and function
200 of the NADH:ubiquinone oxidoreductase (hereafter, “complex I”) of the mitochondrial
201 respiratory chain. Complex I couples electron transport with NADH oxidation and is one of four

202 protein complexes that comprise the electron transport chain (ETC) that generates the
203 electrochemical gradient for ATP biosynthesis. To confirm the GSEA results, we examined the
204 combined dataset for individual genes that make up each complex of the ETC (Figure 2C). This
205 analysis demonstrated that sgRNAs targeting components of complexes II, III or IV had minimal
206 effects on the expression of the IFN γ -inducible surface markers tested. In contrast, the disruption
207 of almost every subunit of complex I impaired the response to IFN γ , with the notable exception
208 of *Ndufab1*. As this gene is essential for viability (93), we assume that cells carrying *Ndufab1*
209 sgRNAs retain functional target protein.

210 To investigate the contribution of specific complex I components to different IFN γ -
211 stimulated phenotypes, we reviewed the surface marker-specific enrichment scores for genes that
212 contribute to the complex assembly, the electron-accepting N-module, or the electron-donating Q
213 module (93-98). Of the 48 individual assembly factors or structural subunits of complex I present
214 in our mutant library, 29 were significantly enriched as positive regulators in the global analysis
215 and were generally required for the induction of all IFN γ -inducible markers (Fig. 2D). The
216 enrichment for each functional module in non-responsive cells was statistically significant.
217 However, not all individual complex I components were equally enriched, which could reflect
218 either differential editing efficiency or distinct impacts on function. To investigate the latter
219 hypothesis, we compared our genetic data with a previous proteomic study that quantified the
220 effect of individual complex I subunits on the stability of the largest subcomplex, the N-module
221 (93). For a given subunit, we found a significant correlation between the magnitude of
222 enrichment in our genetic screen and its effect on the structural stability of the module (Fig. 2E),
223 specifically implicating the activity of complex I in the IFN γ response.

224 To directly test the predictions of the screening data, we used CRISPR to generate
225 individual macrophage lines that were deficient for complex I subunits. We first validated the
226 expected metabolic effects of complex I disruption by comparing the intracellular ATP levels in
227 macrophages carrying non-targeting control sgRNA (sgNTC) with *sgNdufa1* and *sgNdufa2* lines.
228 When cultured in media containing the glycolytic substrate, glucose, all cell lines produced
229 equivalent amounts of ATP (Figure 3A). However, when pyruvate was provided as the sole
230 carbon source, and ATP generation depends entirely upon flux through ETC and oxidative
231 phosphorylation (OXPHOS), both *sgNdufa1* and *sgNdufa2* macrophages contained decreased
232 ATP levels compared to sgNTC cells (Figure 3B). To confirm the glycolytic dependency of
233 complex I mutant macrophages, we grew cells in complete media with glucose and treated with
234 the ATP synthase (complex V) inhibitor, oligomycin, which blocks ATP generation by
235 OXPHOS. While oligomycin reduced ATP levels in sgNTC macrophages, this treatment had no
236 effect in *sgNdufa1* and *sgNdufa2* cells (Supplementary Figure 1A), confirming that these
237 complex I-deficient cells rely on glycolysis for energy generation. IFN γ treatment slightly
238 reduced ATP levels in glucose containing media but did not differentially affect cell lines (Figure
239 3A). Throughout these experiments we found that the *sgNdufa1* mutant showed a greater
240 OXPHOS deficiency than the *sgNdufa2* line.

241 We next compared the response to IFN γ in macrophages lacking *Ndufa1* and *Ndufa2* with
242 those carrying CRISPR-edited alleles of *Ifngr1* or the negative regulator of signaling, *Ptpn2*. As
243 CD40 was found to rely on more complex inputs for expression, which include TNF (Figure 1E),
244 we relied on MHCII and PD-L1 as markers of the IFN γ response for subsequent studies. As
245 expected, and consistent with the genetic screen, we found that the loss of *Ifngr1* or *Ptpn2* either
246 abrogated or enhanced the response to IFN γ , respectively. Also consistent with predictions,

247 mutation of complex I genes significantly reduced the IFN γ -dependent induction of MHCII and
248 PD-L1 compared to sgNTC (Figure 3C-F). The *Ndufa1* mutation that abrogates OXPHOS,
249 reduced MHCII induction to the same level as *Ifngr1*-deficient cells. To confirm these results
250 using an orthologous method we treated cells with the complex I inhibitor, rotenone (99). This
251 treatment caused a dose-dependent inhibition of the IFN γ -induced MHCII expression in sgNTC
252 macrophages (Figure 3G) and had a similar inhibitory effect on the residual IFN γ response in
253 *Ndufa2*-deficient cells. Together these results confirm that complex I is required for the induction
254 of immunomodulatory surface molecules in response to IFN γ .

255 To investigate what aspect of mitochondrial respiration contributes to the IFN γ response,
256 we inhibited different components of the ETC. All inhibitors were used at a concentration that
257 abrogated OXPHOS-dependent ATP generation (Supplementary Figure 1B). The complex V
258 inhibitor, oligomycin, inhibited the IFN γ -induced MHCII expression, albeit to a lesser extent
259 than direct complex I inhibition with rotenone (Figure 3H). This partial effect could reflect an
260 inability to dissipate the proton motive force (PMF), which inhibits electron flux throughout the
261 ETC, including through complex I (100). Carbonyl cyanide m-chlorophenyl hydrazone (CCCP)
262 disrupts mitochondrial membrane potential and OXPHOS while preserving electron flux. CCCP
263 had no effect on the IFN γ response, indicating that ATP generation is dispensable for
264 IFN γ responsiveness and highlighting a specific role for complex I activity.

265 We then altered the media composition to test the sufficiency of mitochondrial respiration
266 to drive IFN γ responses independently from aerobic glycolysis. IFN γ was found to stimulate
267 MHCII expression to a similar degree in macrophages cultured in complete media with glucose
268 as in media containing only pyruvate or citrate, which must be catabolized via mitochondrial
269 respiration (Figure 3H). Inhibition of mitochondrial pyruvate import with the chemical inhibitor,

270 UK5099 (101), abrogated MHCII induction in cultures grown in pyruvate, but not in citrate,
271 which is imported via a UK5099-independent mechanism. Taken together these results suggest
272 that cellular respiration is both necessary and sufficient for maximal expression of the IFN γ -
273 inducible surface markers MHCII and PD-L1.

274

275 **Mitochondrial function is specifically required IFN γ -dependent responses.**

276 The mitochondrial-dependency of the IFN γ response contrasted with the known
277 glycolytic-dependency of Toll-like receptor (TLR) signaling, suggesting that TLR responses
278 would remain intact when complex I was inhibited. Indeed, not only were TLR responses intact
279 in *sgNdufa1* and *sgNdufa2* mutant macrophages, these cells secreted larger amounts of TNF or
280 IL-6 than sgNTC cells in response to the TLR2 ligand, Pam3CSK4. (Figure 4A). Thus, the
281 glycolytic dependency of these cells enhanced the TLR2 response, indicating opposing metabolic
282 dependencies for IFN γ and TLR signaling.

283 Whether the effects of complex I on macrophage responsiveness was the result of
284 reduced mitochondrial respiratory function or secondary to cellular stress responses, such as
285 radical generation, remained unclear. To more directly relate mitochondrial function to these
286 signaling pathways, we created cell lines with reduced mitochondrial mass. Macrophages were
287 continuously cultured in linezolid (LZD), an oxazolidinone antibiotic that inhibits the
288 mitochondrial ribosome (102-104). This treatment produced a cell line with ~50% fewer
289 mitochondrial genomes per nuclear genome and a corresponding decrease in OXPHOS capacity,
290 compared to control cells grown in the absence of LZD (Figure 4B,C). Cells were cultured
291 without LZD for 16 hours and then stimulated with either IFN γ or Pam3CSK4. Consistent with
292 our complex I inhibition studies, we found this reduction in mitochondrial mass nearly abrogated

293 the IFN γ -dependent induction of MHCII (Figure 4D), while the TLR2-dependent secretion of
294 TNF and IL-6 was preserved or enhanced (Figure 4E and 4F). Thus, mitochondrial activity,
295 itself, is necessary for a robust IFN γ response.

296 To further address potential secondary effects of mitochondrial inhibition on the
297 IFN γ response, we investigated the role of known oxygen or nitrogen radical-dependent
298 regulators (Supplementary Figure 1C-G). Inhibition of ROS generation by replacing glucose
299 with galactose (66, 100, 105) had no effect on IFN γ -induced MHCII induction. Similarly,
300 neutralization of cytosolic or mitochondrial radicals with N-acetylcysteine or MitoTempo,
301 respectively, had no effect on MHCII induction either alone or in combination with ETC
302 inhibition. The role of the cytosolic redox sensor, *HIF1 α* (106, 107) was addressed by
303 chemically stabilizing this factor with dimethyloxalylglycine (DMOG). A potential role for nitric
304 oxide production was addressed with the specific NOS2 inhibitor 1400W (60, 66, 108). Neither
305 of these treatments affected IFN γ -induced MHCII cell surface expression in the presence or
306 absence of simultaneous Pam3CSK4, further supporting a direct relationship between
307 mitochondrial respiratory capacity and the IFN γ response.

308

309 **Complex I is specifically required for IFN γ signaling in human cells.**

310 To understand the function of complex I during IFN γ -stimulation in human cells, we used
311 monocyte-derived macrophages (MDM) from peripheral blood of healthy donors. As in our
312 mouse studies, we assessed the response of these cells to IFN γ or Pam3CSK4 by quantifying the
313 abundance of IFN γ -inducible surface markers or cytokines that were optimized for human cells.
314 Since HLA-DR is not strongly induced by IFN γ , we included ICAM1 in addition to CD40 and
315 PD-L1 as surface markers. As seen in the murine model, rotenone inhibited the IFN γ -mediated

316 induction of all three markers (Figure 5A). TLR2 responses were assessed by the production of
317 TNF and IL-1 β . Upon Pam3CSK4 stimulation, rotenone significantly enhanced the secretion of
318 IL-1 β and TNF (Figure 5B). While simultaneous treatment with both IFN γ and Pam3CSK4
319 produced the previously described inhibition of IL-1 β (109), rotenone still did not decrease the
320 production of these TLR2 dependent cytokines. Thus, as we observed in mouse cells, complex I
321 is specifically required for IFN γ signaling in human macrophages.

322

323 **Complex I inhibition reduces IFN γ receptor activity.**

324 To understand how complex I activity was shaping the IFN γ response, we first
325 determined whether its effect was transcriptional or post-transcriptional by simultaneously
326 monitoring mRNA and protein abundance over time. Surface expression of PD-L1 was
327 compared with the gene's mRNA abundance, while the surface expression of MHCII was
328 compared with the mRNA abundance of *Ciita*, the activator of MHCII expression that is initially
329 induced by IFN γ (Figure 6 A,B). In both cases, mRNA induction preceded surface expression of
330 the respective protein. More importantly, both mRNA and protein expression of each marker was
331 diminished to a similar degree in *sgNdufa1* and *sgNdufa2*, compared to *sgNTC* cells. Thus, a
332 deficit in transcriptional induction could account for the subsequent decrease in surface
333 expression observed in complex I deficient cells.

334 IFN γ rapidly induces the transcription of a large number of STAT1 target genes,
335 including IRF1, which amplifies the response. The relative impact of complex I inhibition on the
336 immediate transcriptional response versus the subsequent IRF1-dependent amplification was
337 initially assessed by altering the timing of complex I inhibition. As the addition of rotenone was
338 delayed relative to IFN γ stimulation, the ultimate effect on MHCII expression was diminished

339 (Figure 6C). If rotenone was added more than 4 hours after IFN γ , negligible inhibition was
340 observed by 24 hours, indicating that early events were preferentially impacted by rotenone. To
341 more formally test the role of IRF1, this study was performed in macrophages harboring a
342 CRISPR-edited *Irf1* gene. While the level of MHCII induction was reduced in the absence of
343 IRF1, the relative effect of rotenone addition over time was nearly identical in *sgIrf1* and *sgNTC*
344 cells. Thus, mitochondrial function appeared to preferentially impact the initial transcriptional
345 response to IFN γ upstream of IRF1.

346 Ligand induced assembly of the IFNGR1-IFNGR2 receptor complex results in the
347 phosphorylation and transactivation of janus kinases 1 and 2 (JAK1, JAK2).
348 Autophosphorylation of JAK2 at tyrosine residues 1007/1008 positively regulates this cascade
349 and serves as a marker of JAK2 activation. These activating events at the cytoplasmic domains
350 of the IFNGR receptor complex facilitate STAT1 docking and phosphorylation at tyrosine-701
351 (Y701), a prerequisite for the IFN γ response. Additional STAT1 phosphorylation at serine-727
352 can amplify signaling. To determine if complex I is required for these early signal transduction
353 events, we examined the activation kinetics by immunoblot (Figure 6D). The total abundances of
354 IFNGR1, STAT1, and JAK2, were constant in *sgNTC* and *sgNdufa1* cells in the presence and
355 absence IFN γ -stimulation. While we detected robust phosphorylation of JAK2 Y1007/8, STAT1-
356 Y701, and STAT1-S727 over time following IFN γ treatment in *sgNTC* cells, phosphorylation at
357 all three sites was both delayed and reduced across the time-course in *sgNdufa1* cells. We
358 conclude that the loss of complex I function inhibits receptor proximal signal transduction
359 events.

360

361 **Mitochondrial respiration in antigen presenting cells is required IFN γ -dependent T cell**
362 **activation.**

363 As respiration affected both stimulatory and inhibitory antigen presenting cell (APC)
364 functions, we sought to understand the ultimate effect of mitochondrial function on T cell
365 activation. To this end, we generated myeloid progenitor cell lines from Cas9-expressing
366 transgenic mice that can be used for genome-edited and differentiated into either macrophages or
367 dendritic cells using M-CSF or FLT3L, respectively (110, 111). Macrophages differentiated from
368 these myeloid progenitors demonstrated robust induction of all three markers that were the basis
369 for the IFN γ stimulation screens (Supplementary Figure 2A-C). Further, both the IFN γ -mediated
370 upregulation of these markers and the inhibitory effect of rotenone or oligomycin on their
371 induction were indistinguishable from wild-type primary bone marrow-derived macrophages
372 (Supplementary Figure 2D-F). In both macrophages and in dendritic cells (DCs), the induction of
373 MHCII by IFN γ was inhibited by rotenone and oligomycin (Figure 7A). Unlike macrophages,
374 murine DCs basally express MHCII and these inhibitors only repressed the further induction by
375 IFN γ (Figure 7A,B).

376 Both macrophages and DCs were used to determine if the inhibition of complex I in
377 APCs reduces T cell activation. Both types of APCs were stimulated with IFN γ overnight with or
378 without rotenone before washing cells to remove rotenone and ensure T cell metabolism was
379 unperturbed. APCs were then pulsed with a peptide derived from the *Mycobacterium*
380 *tuberculosis* protein ESAT-6, and co-cultured with ESAT-6-specific CD4⁺ T cells from a TCR
381 transgenic mouse (112). T cell activation was assayed by intracellular cytokine staining for IFN γ .
382 In macrophages, T cell stimulation relied on pretreatment of the APC with IFN γ , as a

383 macrophage line lacking the *Ifngr1* gene was unable to support T cell activation. Similarly,
384 inhibition of complex I in macrophages completely abolished antigen-specific T cell stimulation
385 (Figure 7C). DCs did not absolutely require IFN γ pretreatment to stimulate T cells, likely due to
386 the basal expression of MHCII by these cells. Regardless, rotenone treatment of DC abrogated
387 the IFN γ -dependent increase in T cell stimulation (Figure 7C).

388 To confirm the effects of complex I inhibition on T cell activation using a genetic
389 approach and confirm that complex I inhibition acted in a cell-autonomous mechanism, we
390 generated *Ndufa1* knockout myeloid progenitors (Hox-sg*Ndufa1*). Following differentiation into
391 macrophages, Hox-sg*Ndufa1* demonstrated glycolytic dependence and the inability to generate
392 ATP by OXPHOS compared to control Hox-sgNTC macrophages (Supplementary Figure 2G).
393 Having confirmed the expected metabolic effects of *Ndufa1* loss, Hox-sg*Ndufa1* and Hox-
394 sgNTC macrophages were mixed at various ratios. Mixed cultures were then stimulated with
395 IFN γ , peptide pulsed, and co-cultured with antigen-specific CD4⁺ T cells. In agreement with our
396 chemical inhibition studies, we found strong correlation between complex I activity in the APC
397 population and T cell stimulatory activity (Figure 7D-E). Together, these data confirm that the
398 IFN γ -dependent augmentation of T cell stimulatory activity depends on complex I function in
399 both macrophages and DCs.

400

401 **Discussion**

402 IFN γ -mediated control of APC function is central to shaping a protective immune
403 response, and the canonical IFN γ signal transduction pathway has been elucidated in exquisite
404 detail (113). Our study demonstrates that unbiased genetic analyses can reveal a multitude of
405 unexpected cellular regulators, even for a well-characterized process such as IFN γ signaling. By

406 independently assessing genetic determinants of stimulatory and inhibitory molecule expression,
407 we discovered mechanisms of regulation that preferentially affect the induction of different cell
408 surface proteins. These results begin to explain how a single cytokine can induce functionally
409 distinct downstream responses in different contexts. These data also suggest new strategies to
410 modulate individual co-receptors to either stimulate or inhibit T cell activation. Another strength
411 of our parallel screen approach was the increased power to identify shared mechanisms that
412 control IFN γ -mediated regulation across all screens. Our pooled analysis identified
413 mitochondrial respiration, and in particular complex I, as essential for IFN γ -responses in APCs.
414 We determined that complex I is required for the IFN γ -mediated induction of key immune
415 molecules and is necessary for antigen presentation and T cell activation. These findings uncover
416 a new dependency between cellular metabolism and the immune response.

417 Our genetic and chemical inhibition data demonstrated that mitochondrial respiration is
418 necessary for early events in signal transduction from the IFN γ receptor complex, and complex I
419 of the respiratory chain is specifically required. While IFN γ stimulation has been reported to
420 mediate a reduction in oxygen consumption and a shift to aerobic glycolysis over time (66), the
421 requirement of mitochondrial respiration in IFN γ responses has not been assessed previously.
422 Our results indicate that complex I is required for IFN γ signaling regardless of these metabolic
423 shifts. Complex I is a metabolic hub with several core functions that cumulatively recycle
424 nicotinamide adenine dinucleotide (NAD⁺), reduce ubiquinol, and initiate the PMF for ATP
425 generation. While any or all of these physiologic processes could contribute to IFN γ signaling,
426 the differential effects of chemical inhibitors narrow the possibilities. Both rotenone and
427 oligomycin inhibit the IFN γ response, and block electron flux through complex I either directly
428 or indirectly. In contrast, the ionophore CCCP disrupts the PMF and ATP generation without

429 inhibiting electron transfer, and does not affect IFN γ signaling. These data indicate that the
430 reduction state of the quinone pool and ATP generation do not regulate IFN γ responses in our
431 system. Instead, complex I-dependent regeneration of NAD⁺ is the most likely regulator of IFN γ
432 signaling. Indeed, NAD⁺ synthesis via either the *de novo* or salvage pathway is necessary for a
433 variety of macrophage functions (114-116). Very recent work demonstrates an important role for
434 NAD⁺ in STAT1 activation and PD-L1 induction by IFN γ in hepatocellular carcinoma cells
435 (117). In this setting, inhibition of NAD⁺ synthesis reduces the abundance of phospho-STAT1
436 by disrupting a direct interaction with the Ten-eleven translocation methylcytosine dioxygenase
437 1 (TET1). It remains unclear if a similar interaction occurs in the myeloid cells that are the focus
438 of our work, as TET1 is expressed at very low levels in macrophages and splenic DC (118).
439 Regardless, these observations indicate that both NAD⁺ synthesis and its regeneration via
440 mitochondrial respiration contribute to the IFN γ response in diverse cell types. This recently
441 revealed interaction between metabolism and immunity could contribute to the observed
442 association between NAD⁺ homeostasis and inflammatory diseases (116), as well as the efficacy
443 of checkpoint inhibitor therapy for cancer (117).

444 In the APC setting, we found that T cell activation required mitochondrial respiration.
445 While complex I function, MHCII and CD40 expression all largely correlate with T cell
446 stimulation, our data indicate that additional IFN γ -inducible pathways also contribute to this
447 activity. For example, unstimulated DCs basally express similar levels of MHCII as IFN γ -
448 stimulated macrophages but are unable to productively present antigen to T cells. This
449 observation suggests that additional aspects of antigen processing, presentation, or co-stimulation
450 are IFN γ - and complex I-dependent. Similarly, MHCI presentation machinery is transcriptionally
451 induced upon IFN γ stimulation (7, 119) and the induction of molecules recognized by donor

452 unrestricted T cells, such as MR1 and CD1, might also require additional signals to function. The
453 specific effects of mitochondrial respiration on the type and quality of the T cell response will
454 depend on how these diverse antigen-presenting and co-signaling molecules are influenced by
455 cellular metabolic state.

456 The observation that IFN γ signaling depends on mitochondrial respiration provides a
457 stark contrast to the well-established glycolytic dependency of many phagocyte functions, such
458 as TLR signaling. This metabolic dichotomy between proinflammatory TLR signals and the
459 IFN γ response mirrors known regulatory interactions between these pathways. For example,
460 TLR stimulation has been shown to inhibit subsequent IFN γ responses, via a number of target
461 gene-specific mechanisms (120-124). However, TLR stimulation also results in the disassembly
462 of the ETC (123, 124), which our observations predict to inhibit STAT1 phosphorylation and
463 IFN γ signaling at the level of the receptor complex. More generally, our work suggests
464 fundamental metabolic programs contribute to the integration of activation signals by APC and
465 influence the ultimate priming of an immune response.

466

467 **Materials and Methods**

468 **Cell culture**

469 Cells were cultured in Dulbecco's Modified Eagle Medium (Gibco 11965118) supplemented
470 with 10% fetal bovine serum (Sigma F4135), sodium pyruvate (Gibco 11360119), and HEPES
471 (15630080). Primary bone marrow-derived macrophages (BMDMs) were generated by culturing
472 bone marrow in the presence of media supplemented with 20% L929 supernatant for 7 days.

473

474 Immortalized macrophage cell lines in C57Bl6/J and Cas9-EGFP were established in using J2
475 retrovirus from supernatant of CREJ2 cells as previously described(125). Briefly, isolated bone
476 marrow was cultured in the presence of media enriched with 20% L929 supernatant. On day 3,
477 Cells were transduced with virus and cultured with virus for 2 days. Over the next 8 weeks, L929
478 media was gradually reduced to establish growth factor independence.

479

480 Conditionally immortalized myeloid progenitor cell lines were generated by retroviral
481 transduction using an estrogen-dependent Hoxb8 transgene as previously described(110).
482 Briefly, mononuclear cells were purified from murine bone marrow using Ficoll-Paque Plus (GE
483 Healthcare 17144002) and cultured in RPMI (Gibco 11875119) containing 10% fetal bovine
484 serum (Sigma F4135), sodium pyruvate (Gibco 11360119), and HEPES (15630080), IL-6
485 (10ng/mL; Peprotech #216-16), IL-3 (10ng/mL; Peprotech #213-13), and SCF (10ng/mL;
486 Peprotech #250-03) for 48 hours. Non-adherent bone marrow cells from C57Bl6/J (Jax 000664),
487 Cas9-EGFP knockin (Jax 026179), or Ifngr1 knockout (Jax 003288) mice were transduced with
488 ER-Hoxb8 retrovirus. After transduction cells were cultured in with media supplemented with
489 supernatant from B16 cells expressing GM-CSF and 10uM estradiol (Sigma E8875) to generate
490 macrophage progenitor cell lines or in media supplemented with supernatant from B16 cells
491 expressing FLT3L and 10uM estradiol (Sigma E8875) to generate dendritic cell progenitor lines.
492 To differentiate macrophages, progenitors were harvested and washed twice with PBS to remove
493 residual estradiol and cultured in L929 supplemented media as above. To differentiate dendritic
494 cells(111), progenitors were harvested, washed 2x with PBS, and cultured in FLT3-enriched
495 complete RPMI for 8-10 days.

496

497 Human monocyte-derived macrophages (MDM) were differentiated from mononuclear cells of
498 healthy donors. Briefly, peripheral blood mononuclear cells (PBMCs) were isolated from whole
499 blood using Ficoll-Paque-PLUS (GE Healthcare 17144002). CD14⁺ monocytes were purified
500 using MojoSort™ Human CD14 Nanobeads (Biolegend 480093) according to the manufacturer's
501 protocol. Cells were cultured in RPMI with 10% FBS, sodium pyruvate, and HEPES and
502 supplemented with recombinant GM-CSF (50ng/mL, Peprotech 300-03) for 6 days. Thaws were
503 harvested using Accutase (Gibco A1110501).

504

505 **Cell stimulations**

506 Murine IFN γ (Peprotech 315-05) and human IFN γ (Peprotech 300-02) were used at 10ng/mL
507 unless otherwise indicated in the figure legends. Murine TNF (315-01A) was used at 25ng/mL.
508 Pam3CSK4 (Invivogen tlrl-pms) was used at 200ng/mL.

509

510 **CRISPR screens**

511 A clonal macrophage cell line stably expressing Cas9 (L3) was established as described
512 elsewhere(79). A plasmid library of sgRNAs targeting all protein coding genes in the mouse
513 genome (Brie Knockout library, Addgene 73633) was packaged into lentivirus using HEK293T
514 cells. HEK293T supernatants were collected and clarified, and virus was titered by quantitative
515 real-time PCR and by colony counting after transduction of NIH3T3. L3 cells were transduced at
516 a multiplicity of infection (MOI) of ~0.2 and selected with puromycin 48 hours after
517 transduction (2.5ug/mL). The library was minimally expanded to avoid skewing mutant
518 representation and then frozen in aliquots in freezing media (90% FBS 10% DMSO).

519

520 Two replicate screens for MHCII, CD40, and PD-L1 were performed as follows:
521 2e8 cells of the knockout (KO) library was stimulated with IFN γ (10ng/mL; Peprotech 315-05)
522 for 24 hours after which cells were harvested by scraping to ensure integrity of cell surface
523 proteins. Cell were stained with TruStain FcX anti-mouse CD16/32 (Biolegend 101319) and
524 LIVE/DEAD Fixable Aqua (Invitrogen L34957) per the manufacturer's instructions. For each of
525 the respective screens, stimulated library was stained for its respective marker with the following
526 antibody: MHCII (APC anti-mouse I-A/I-E Antibody, Clone M5/114.15.2 Biolegend 107613),
527 CD40 (APC anti-mouse CD40 Antibody, Clone 3/23 Biolegend 124611), or PD-L1 (APC anti-
528 mouse CD274 (B7-H1, PD-L1) Antibody, Clone 10F.9G2 Biolegend 124311). Each antibody
529 was titrated for optimal staining using the isogenic L3 macrophage cell line. Following staining,
530 cells were fixed in 4% paraformaldehyde. High and low expressing populations were isolated by
531 fluorescence activated cell sorting (FACS) using a BD FACS Aria II Cell Sorter. Bin size was
532 guided by control cells which were unstimulated and to ensure sufficient library coverage (>25x
533 unselected library, or >2e6 cells per bin). Following isolation of sorted populations,
534 paraformaldehyde crosslinks were reversed by incubation in proteinase K (Qiagen) at 55 degrees
535 for 6-8 hours. Subsequently, genomic DNA was isolated using DNeasy Blood and Tissue Kit
536 (Qiagen 69504) according to the manufacturer's instructions. Amplification of sgRNAs by PCR
537 was performed as previously described(74, 126) using Illumina compatible primers from IDT,
538 and amplicons were sequenced on an Illumina NextSeq500. Sequence reads were trimmed to
539 remove adapter sequence and to adjust for staggered forward (p5) primer using Cutadapt v2.9.
540 Raw sgRNA counts for each sorted and unsorted (input library) population was quantified using
541 bowtie2 via MAGeCK to map reads to the sgRNA library index (no mismatch allowed); a
542 sgRNAindex was modified to reflect genes transcribed by our macrophage cell line either basally

543 or upon stimulation with IFN γ as previously published(79). Counts for sgRNAs were median
544 normalized to account for variable sequencing depth.

545

546 **MAGeCK-MLE**

547 We used MAGeCK-MLE to test for gene enrichment. Two separate analyses were performed in
548 order to: (1) identify regulators of the IFN γ response, and (2) identify specific regulators of each
549 of the screen targets. For both analyses, the baseline samples were the input libraries from each
550 of the replicate screens in order to account for slight variabilities in library distribution for each
551 screen. For (1), the generalized linear model was based on a design matrix that was "marker-
552 blind" and only considered the bin of origin (i.e. MHCII-low, CD40-low, PD-L1-low v. MHCII-
553 high, CD40-high, PD-L1-high). For (2), the design matrix was "marker-aware and bin-specific"
554 to test for marker-specific differences (i.e. MHCII-low v. CD40-low v. PD-L1-low); the analysis
555 was performed separately for each bin, low or high expressing mutants, to identify marker-
556 specific positive and negative regulators, respectively. For each analysis, β scores (selection co-
557 efficient) for each gene were summed across conditions to allow for simultaneous assessment of
558 positive and negative regulators across conditions. Data are provided in Supplementary Tables.

559

560 Gene-set enrichment analysis (GSEA) was performed using a ranked gene list as calculated from
561 MAGeCK-MLE beta scores and false discovery rate (FDR). To facilitate the identification of
562 positively and negatively enriched gene sets from the high and low expressing populations, the
563 positive ("pos | beta") and negative ("neg | beta") beta scores for each gene were summed as
564 described above ("beta_sum"). To generate a ranked gene list for GSEA, we employed
565 Stouffer's method to sum positive ("pos | z") and negative ("neg | z") selection z-scores, which

566 were used to re-calculate p-values (“p_sum”) as has been previously described (127-129). Using
567 these summative metrics, we calculated a gene score as: $\log_{10}(p_sum) * (beta_sum)$. Genes were
568 ranked in descending order and GSEA was performed with standard settings including
569 “weighted” enrichment statistic and “meandiv” normalization mode. Analysis was inclusive of
570 gene sets comprising of 10-500 genes that were compiled and made available online by the
571 Bader lab (130, 131).

572

573 **Plasmids and sgRNA cloning**

574 Lentivirus was generated using HEK293T cells using packaging vector psPAX2
575 (Addgene#12260) and envelope plasmid encoding VSV-G. Transfections used TransIT-293
576 (MirusBio MIR 2704) and plasmid ratios according to the manufacturer's instructions. For the
577 generation of retrovirus, pCL-Eco in place of separate packaging and envelope plasmid.
578 Retrovirus encoding the ER-Hoxb8 transgene was kindly provided by David Sykes.

579

580 sgOpti was a gift from Eric Lander & David Sabatini (Addgene plasmid #85681)(132).
581 Individual sgRNAs were cloned as previously described. Briefly, annealed oligos containing the
582 sgRNA targeting sequence were phosphorylated and cloned into a dephosphorylated and BsmBI
583 (New England Biolabs) digested SgOpti (Addgene#85681) which contains a modified sgRNA
584 scaffold for improved sgRNA-Cas9 complexing. Use of sgOpti derivatives for delivery of
585 multiple sgRNAs was performed as detailed elsewhere(79). The sgRNA targeting sequences
586 used for cloning were as follows:

Name/Target	sgRNA sequence
sglfngr1_1	TATGTGGAGCATAACCGGAG
sglfngr1_2	GGTATTCCCAGCATACGACA
sglrf1_1	CTGTAGGTTATACAGATCAG

sgIrf1_2 CGGAGCTGGGCCATTACAC
sgPtpn2_1 AAGAAGTTACATCTTAACAC
sgPtpn2_2 TGCAGTGATCCATTGCAGTG
sgNdufa1_1 TGTACGCAGTGGACACCCCG
sgNdufa1_2 CGCGTTCCATCAGATACCAC
sgNdufa2_1 GCAGGGATTTTCATCGTGCAA
sgNdufa2_2 ATTCGCGGATCAGAATGGGC
sgStat1_1 GGATAGACGCCAGCCACTG
sgStat1_2 TGTGATGTTAGATAAACAGA
sgOstc_1 GCGTACACCGTCATAGCCGA
sgOstc_2 TCTTACTTCTCATTACCGG
sgCnbp_1 AGGTAAAACCACCTCTGCCG
sgCnbp_2 GTTGAAGCCTGCTATAACTG

587

588 **Flow cytometry**

589 Cells were harvested at the indicated times post-IFN γ stimulation by scrapping to ensure intact
590 surface proteins. Cells were pelleted and washed with PBS before staining with TruStain FcX
591 anti-mouse CD16/32 (Biolegend 101319) or TruStain FcX anti-human (Biolegend 422301) and
592 LIVE/DEAD Fixable Aqua (Invitrogen L34957) per the manufacturer's instructions. The
593 following antibodies were used as indicated in the figure legends:

594 APC-Fire750 anti-mouse I-A/I-E Antibody, Clone M5/114.15.2 Biolegend 107651

595 PE anti-mouse CD40 Antibody, Clone 3/23 Biolegend 124609

596 Brilliant Violet 421TM anti-mouse CD274 (B7-H1, PD-L1) Antibody, Clone 10F.9G2 Biolegend
597 124315

598 Alexa Fluor[®] 647 anti-human CD54 Antibody, Clone HCD54, Biolegned 322718

599 PE anti-human CD40 Antibody, Clone 5C3, Biolegned 334307

600 Brilliant Violet 421TM anti-human CD274 (B7-H1, PD-L1) Antibody, Clone 29E.2A3, Biolegend
601 329713

602 APC/FireTM 750 anti-human HLA-DR Antibody, Clone L243, Biolegend 307657

603

604 For intracellular cytokine staining, cells were treated with brefeldin A (Biolegend 420601) for 5
605 hours before harvesting. Following staining and fixation, cells were permeabilized (Biolegend
606 421002) and stained according to the manufacturer's protocol using the following antibodies:

607 PE anti-mouse IFN- γ Antibody, Biolegend 505807

608

609 Surface protein expression was analyzed on either a MacsQuant Analyzer or Cytex Aurora. All
610 flow cytometry analysis was done in FlowJo V10 (TreeStar).

611

612 **Chemical inhibitors**

613 All chemical inhibitors were used for the duration of cell stimulation unless otherwise stated.

614 Rotenone (Sigma R8875) was resuspended in DMSO and used at 10uM unless indicated

615 otherwise in the figure legend. Oligomycin (Cayman 11342) was resuspended in DMSO and

616 used at 2.5uM unless otherwise indicated. CCCP (Cayman 25458) was resuspended in DMSO

617 and used at 1.5uM unless indicated otherwise. 1400W hydrochloride (Cayman 81520) was

618 resuspended in culture media, filter sterilized and used immediately at 25uM unless otherwise

619 indicated. N-acetyl-L-Cysteine (NAC, Cayman 20261) was resuspended in culture media, filter

620 sterilized and used immediately at 10mM. DMOG (Cayman 71210) was resuspended in DMSO

621 and used at 200uM. UK5099 (Cayman 16980) was resuspended in DMSO and used at 20uM. 2-

622 deoxy-D-Glucose (2DG, Cayman 14325) was resuspended in culture media, filter sterilized and

623 used at 1mM or at the indicated concentrations immediately. MitoTEMPO hydrate (Cayman

624 16621) was resuspended in DMSO and used at the indicated concentrations.

625

626 For experiments that used defined minimal media with carbon supplementation, D-galactose,
627 sodium pyruvate, and D-glucose were used at 10mM in DMEM without any carbon (Gibco
628 A1443001). For establishment of macrophage cell line with diminished mitochondrial mass,
629 cells were continuously cultured in linezolid (LZD) (Kind gift from Clifton Barry) for 4 weeks at
630 50 µg/mL or DMSO control. Both LZD-conditioned and DMSO control lines were
631 supplemented with uridine at 50 µg/mL. Prior to experimentation, cells were washed with PBS
632 and cultured without linezolid for at least 12 hours.

633

634 **ELISA and nitric oxide quantification**

635 The following kits were purchased from R and D Systems or Biolegend for quantifying protein
636 for cell supernatants:

637 Mouse IL-6 DuoSet ELISA (DY406) or Biolegend ELISAmax (431301)

638 Mouse TNF-alpha DuoSet ELISA (DY410) or Biolegend ELISAmax (430901)

639 Mouse IFN-gamma DuoSet ELISA (DY485)

640 Human IL-1 beta/IL-1F2 DuoSet ELISA (DY201)

641 Human TNF-alpha DuoSet ELISA (DY210)

642 Nitric oxide was quantified from cell supernatants using the Griess Reagent System according to
643 the manufacturer's instructions (Promega G2930). For these experiments, cell culture media
644 without phenol red (Gibco A1443001 or Gibco 31053028).

645

646 **RNA isolation and quantitative real-time PCR**

647 To isolate RNA, cells were lysed in TRIzol (15596026) according to manufacturer's instructions.

648 Chloroform was added to lysis at ratio of 200uL chloroform per 1mL TRIzol and centrifuged at

649 12,000 x g for 20 minutes at 4C. The aqueous layer was separated and added to equal volume of
650 100% ethanol. RNA was isolated using the Zymo Research Direct-zol RNA extraction kit.
651 Quantity and purity of the RNA was checked using a NanoDrop and diluted to 5ng/uL in
652 nuclease-free water before use. Quantitative real-time PCR was performed using NEB Luna®
653 Universal One-Step RT-qPCR Kit (E3005) or the Quantitect SYBR green RT-PCR kit (204243)
654 according to the manufacturer's protocol and run on a Viia7 thermocycler or StepOne Plus
655 Thermocycler. Relative gene expression was determined with ddCT method with beta-Actin
656 transcript as the reference.

Primer	Sequence
RT_Actb-1F	GGCTGTATTCCCCTCCATCG
RT_Actb-1R	CCAGTTGGTAACAATGCCATGT
RT_Cd274-1F	GCTCCAAAGGACTTGTACGTG
RT_Cd274-1R	TGATCTGAAGGGCAGCATTTC
RT-Ciita-1F	AGACCTGGATCGTCTCGT
RT-Ciita-1R	AGTGCATGATTTGAGCGTCTC
RT-Gapdh-1F	TGGCCTTCCGTGTTCCCTAC
RT-Gapdh-1R	GAGTTGCTGTTGAAGTCGCA

657

658 **Quantification of mitochondrial genomes**

659 Genomic DNA was isolated from cell pellets using the DNeasy Blood and Tissue Kit (Qiagen
660 69504). Quantitative PCR was run using NEB Luna® Universal One-Step RT-qPCR without the
661 RT enzyme mix and run on a Viia7 thermocycler. Relative quantification of mitochondrial
662 genomes was determined by measuring the relative abundance of mitochondrially encoded gene
663 Nd1 to the abundance of nuclear encoded Hk2 as has been described elsewhere(133). All primers
664 are detailed in attached table.

665

Name/Target	Sequence
Mm-Nd1-1F	CTAGCAGAAACAAACCGGGC
Mm-Nd1-1R	CCGGCTGCGTATTCTACGTT
Mm-Hk2-1F	GCCAGCCTCTCCTGATTTTAGTGT
Mm-Hk2-1R	GGGAACACAAAAGACCTCTTCTGG

666

667 **Immunoblot**

668 At the indicated times following stimulation, cells were washed with PBS once and lysed in on
669 ice using the following buffer: 1% Triton X-100, 150mM NaCl, 5mM KCl, 2mM MgCl₂, 1mM
670 EDTA, 0.1% SDS, 0.5% DOC, 25mM Tris-HCl, pH 7.4, with protease and phosphatase inhibitor
671 (Sigma #11873580001 and Sigma P5726). Lysates were further homogenized using a 25g needle
672 and cleared by centrifugation before quantification (Pierce™ BCA Protein Assay Kit, 23225).

673 Parallel blots were run with the same samples, 15ug per well. The following antibodies were
674 used according to the manufacturer's instructions:

675 Purified anti-STAT1 Antibody Biolegend Clone A15158C

676 Purified anti-STAT1 Phospho (Ser727) Antibody, Biolegend Clone A15158B

677 Phospho-Stat1 (Tyr701) Rabbit mAb, Cell Signaling Technology Clone 58D6

678 Jak2 XP® Rabbit mAb, Cell Signaling Technology Clone D2E12

679 Phospho-Jak2 (Tyr1007/1008) Antibody, Cell Signaling Technology #3771S

680 Anti-mouse β-Actin Antibody, Santa Cruz Biotechnology Clone C4

681 Biotin anti-mouse CD119 (IFN-γ R α chain) Antibody, Biolegend Clone 2E2

682 Goat anti-Rabbit IgG (H+L) Secondary Antibody, HRP, Invitrogen 31460

683 Goat anti-Mouse IgG (H+L) Secondary Antibody, HRP, Invitrogen 31430

684 HRP-Conjugated Streptavidin, Thermo Scientific N100

685

686 **Bioenergetics Assay**

687 Relative glycolytic and respiratory capacity were determined as has previously been
688 demonstrated(134). Briefly, cellular ATP levels were determined using CellTiter-Glo® 2.0 Cell
689 Viability Assay (Promega G9241) according to the manufacturer's protocol. Cells were grown in
690 the conditions indicated in the figure legends for 4 hours unless stated otherwise. ATP levels
691 were normalized according to the figure legend.

692

693 **T cell activation assay**

694 We used a previously established co-culture system to assess antigen presentation to Ag-specific
695 T cells. Briefly, C7 CD4⁺ T cells were isolated from transgenic C7 mice, respectively and
696 stimulated in vitro with irradiated splenocytes pulsed with the ESAT-61-15 peptide, in complete
697 media (RPMI with 10% FBS) containing IL-2 and IL-7. After the initial stimulation, the T cells
698 were split every two days for 3-4 divisions and rested for two to three weeks. After the initial
699 stimulation, the cells were cultured in complete media containing IL-2 and IL-7. The following
700 synthetic peptide epitopes were used as antigens from New England Peptide (Gardener, MA):
701 ESAT-61-15 (MTEQQWNFAGIEAAA).

702 For use in co-culture assay, T cells were added to peptide-pulsed macrophages as described in
703 figure legends at an effector to target ratio of 1:1. Following 1 hours of co-culture, brefeldin A
704 was added for 5 hours before assessing intracellular cytokine production by ICS.

705

706 **Quantification of subunit effects on N-module**

707 We used publicly available proteomics data in which the protein abundance of all complex I
708 subunit was measured when each subunit was genetically deleted(93). As determined empirically

709 by the authors, the N-module components included: NDUFA1, NDUFA2, NDUFS1, NDUFV2,
710 NDUFA6, NDUFS6, NDUFA7, NDUFS4, and NDUFV3. The relative effect of each subunit
711 (using a knockout of that subunit) on N-module protein stability was calculated as the sum of the
712 median log₂ ratio of each of the above mentioned subunits, minus the median log₂ ratio of itself
713 (since it is knocked out).

714

715 **Statistical Analysis and Figures**

716 Statistical analysis was done using Prism Version 8 (GraphPad) as indicated in the figure
717 legends. Data are presented, unless otherwise indicated, as the mean +/- the standard deviation.
718 Figures were created in Prism V8 or R (Version 3.6.2). MAGeCK-MLE was used as part of
719 MAGeCK-FLUTE package v1.8.0.

720

721 **Acknowledgements**

722 We thank all the members of the Sasseti, Behar, and Olive labs for critical feedback and input
723 throughout the project. A special thank you to Megan K. Proulx, Mario Meza Segura and the
724 donors for their assistance and expertise to the human macrophage derivation We thank the flow
725 cytometry core at UMMS for their help in all experiments requiring flow cytometry. This work
726 was supported by startup funding to AJO provided by Michigan State University, support from
727 the Arnold O. Beckman Postdoctoral fellowship to AJO and grants from the NIH (AI146504,
728 AI132130), DOD (W81XWH2010147), and USDA (NIFA HATCH 1019371). All data is being
729 deposited into the appropriate databases and is available upon request.

730

731 **Competing Interests**

732 The authors have no competing interests related to the research described in this manuscript.

733

734 **Figure Legends:**

735 **Figure 1. Forward genetic screen to identify regulators of the IFN γ response. A)**

736 Representative histograms of the three selected cell surface markers targeted in macrophage
737 CRISPR screens: MHCII, CD40, and PD-L1. Blue histograms indicate expression of each
738 marker in unstimulated macrophages and alternatively colored histograms show expression
739 following 24 hour stimulation with recombinant murine IFN γ (10ng/mL). Gates used for sorting
740 “high” and “low” populations are shown. B) Schematic of CRISPR screens. C) Relative
741 enrichment of select positive control (points) and all 1000 non-targeting control sgRNAs (gray
742 distribution) are plotted as a function of their log₂ fold enrichment (“high” vs “low” bins). Data
743 are from both replicate selections for each sgRNA (sgRNA denoted by shape). D) Heatmap of β
744 scores from CRISPR analysis, ordered according to k-means clustering (k=8) of the 5% most
745 enriched or depleted genes in each screen. E) Macrophages were stimulated for 24 hours with
746 TNF (25ng/mL), IFN γ (10ng/mL) or both TNF and IFN γ . Mean fluorescence intensity (MFI) of
747 CD40 and MHCII were quantified by flow cytometry. Data are mean \pm the standard deviation for
748 3 biological replicates. Representative scatter plot from two independent experiments is
749 provided. F) Macrophages transduced with sgRNA targeting *Stat1*, *Ostc*, *Cnbp*, or a NTC control
750 were cultured with or without IFN γ for 24 hours and cell surface expression of PD-L1 (MFI) was
751 quantified by flow cytometry. For each genotype, data are the mean of cell lines with two
752 independent sgRNAs \pm the standard deviation. Data are representative of three independent
753 experiments. Statistical testing in panel C was performed with Tukey’s multiple comparisons
754 test. Within each screen, the sgRNA effects for each gene were compared to the distribution non-
755 targeting control sgRNAs. Statistical testing in panels E and F was performed by one-way

756 ANOVA with Holm-Sidak multiple comparisons correction. p values of 0.05, 0.01, 0.001, and
757 0.001 are indicated by *, **, ***, and ****

758

759 **Figure 2. Global analysis of knockout libraries implicates mitochondrial complex I is a**
760 **positive regulator of the IFN γ response.** A) Rank plot of the combined analysis for all genome-
761 wide knockout screens. Gene ranks (x-axis) were determined by maximal likelihood estimation
762 (MLE). Known positive (left) and negative (right) regulators of IFN γ -mediated signaling are
763 highlighted. The q-value (false discovery rate) for each gene is indicated by dot size ($-\text{Log}_{10}$
764 FDR). B). Gene set enrichment analysis (GSEA) is based on the ranked list of positive
765 regulators. Non-redundant pathways with a normalized enrichment score (NES) exceeding 2.0
766 and a false discovery rate (FDR) below 0.025 are labeled. C) Relative enrichment (log₂ fold
767 change between “high” and “low” bins) of genes which comprise the mitochondrial respirasome
768 (GeneOntology 0005746) and were targeted in the CRISPR KO library. Respirasome
769 components are grouped by ETC complex. FDR is based on MAGeCK-MLE. D) Screen-specific
770 enrichment score is plotted for Complex I structural subunits and assembly factors. The
771 statistical enrichment of a gene (e.g. *Ndufa1*) or module (e.g. N) was calculated using a binomial
772 distribution function to calculate the probability that observed sgRNAs under examination would
773 be depleted or enriched given the expected median probability. P values of 0.05, 0.01, 0.001, and
774 0.001 are indicated by *, **, ***, and ****. E) Correlation between the relative effect of each
775 complex I subunit on the structural integrity of the N-module (x-axis) with the relative
776 requirement of each complex I subunit for the IFN γ -response (y-axis; β score, as in Panel D).
777 The Pearson correlation coefficient (r) was calculated to be 0.6452 (95% confidence interval
778 0.3584 to 0.8207; p-value = 0.0002. As *Ndufab1* (empty square) is an essential gene, its

779 detection in the library indicates editing did not eliminate function; therefore, it was excluded
780 from correlation analysis.

781

782 **Figure 3. Complex I is necessary for IFN γ -induced MHCII and PD-L1 expression.**

783 Metabolic phenotypes in macrophage mutants were confirmed using ATP abundance following
784 culture in media containing only (A) glucose or (B) pyruvate. Values are normalized to the
785 average respiratory capacity of non-targeting control macrophages (NTC) and are the mean \pm the
786 standard deviation for 4 biological replicates. Statistical testing within each condition (with or
787 without IFN γ for 24h) was performed by one-way ANOVA with Dunnett's multiple comparisons
788 correction. (C-F) Non-targeting control (NTC), positive control (*sgIfngr1* and *sgPtpn2*) and
789 complex I mutant (*sgNdufa1* and *sgNdufa2*) macrophages were stimulated for 24 hours with
790 recombinant murine IFN γ . Plotted values in C and E are the geometric mean fluorescence
791 intensity (MFI) for a given mutant normalized to an internal control present in each well; for
792 each gene, the data are the mean for two independent sgRNAs \pm the standard deviation.
793 Representative histograms are provided in D and F. Data are representative of >5 independent
794 experiments. G) MHCII MFI of macrophages stimulated with IFN γ and treated with rotenone at
795 the indicated concentrations for 24 hours. Mean \pm the standard deviation for 2 biological
796 replicates are shown. Data are representative of four independent experiments. H) Left: MHCII
797 MFI on macrophages cultured in complete media (CM) and stimulated with IFN γ and the
798 indicated inhibitors for 24 hours. Right: MHCII MFI on macrophages cultured in CM or media
799 containing only pyruvate (Pyr) or citrate (Cit) with or without UK5099 and stimulated with
800 IFN γ for 24 hours. Mean \pm standard deviation for 2 or 3 biological replicates is indicated. Data
801 are representative of four independent experiments. Statistical testing was performed by one-way

802 ANOVA with Tukey correction for multiple hypothesis testing. p values of 0.05, 0.01, 0.001,
803 and 0.001 are indicated by *, **, ***, and ****.

804

805 **Figure 4. Diminished mitochondrial function specifically limits IFN γ -dependent responses.**

806 A) TNF and IL-6 production by NTC or complex I mutant macrophages stimulated with
807 Pam3CSK4 for 24 hours was determined by ELISA. Statistical testing between mutant and NTC
808 macrophages from triplicate samples was performed by ANOVA with Dunnett's correction for
809 multiple comparisons. Data are representative of two independent experiments. B) qPCR
810 determination of relative mitochondrial genomes present per nuclear genome in macrophages
811 cultured in vehicle (WT) or 50 ug/mL linezolid (LZD). C_t values were normalized to reference
812 nuclear gene hexokinase 2 (*Hk2*) and plotted as abundance relative to WT. Data were analyzed
813 by two-way unpaired t-test. C) ATP abundance in control or LZD-conditioned macrophages
814 cultured in 10mM glucose, galactose or pyruvate. ATP values normalized to mean of 10mM
815 glucose and plotted as percent. Mean \pm the standard deviation for 2 biological replicates of each
816 condition. Differences were tested by two-way ANOVA using the Sidak method to correct for
817 multiple hypothesis testing. D) MFI of MHCII was determined by flow cytometry on control or
818 LZD-conditioned macrophages following 24 hour stimulation with IFN γ . Mean \pm the standard
819 deviation for 2 biological replicates of each condition and representative of two independent
820 experiments. Differences were tested by two-way ANOVA using the Tukey method to correct
821 for multiple hypothesis testing. E and F) Secretion of TNF and IL-6 in WT and LZD-conditioned
822 macrophages following Pam3CSK4 stimulation for 6 hours was quantified by ELISA. Mean \pm
823 the standard deviation for 3 biological replicates of each condition and two independent

824 experiments. Data were analyzed by two-way unpaired t-test. p values of 0.05, 0.01, 0.001, and
825 0.001 are indicated by *, **, ***, and ****.

826

827 **Figure 5. Complex I is specifically required for IFN γ signaling in human cells.** A) CD14+
828 monocytes from healthy human donors were differentiated into macrophages. MFI of cell
829 surface markers PD-L1, ICAM1, CD40 and HLA-DR was determined by flow cytometry
830 following stimulation with IFN γ and/or inhibition of complex I with rotenone (10 μ M) for 24
831 hours. Data are representative of two independent experiments and values are normalized to
832 donor-specific unstimulated/vehicle control. Mean \pm the standard deviation for 6 biological
833 replicates of each condition. Differences were tested by two-way ANOVA using the Sidak-Holm
834 method to correct for multiple hypothesis testing. B and C) Quantification of IL-1 β and TNF
835 production from primary human macrophages, measured by ELISA from cell supernatants
836 following stimulation. Lines connect values for individual donors treated with vehicle (DMSO,
837 black squares) or rotenone (empty squares). Differences were tested by repeat-measure two-way
838 ANOVA using the Sidak-Holm method to correct for multiple hypothesis testing. p values of
839 0.05, 0.01, 0.001, and 0.001 are indicated by *, **, ***, and ****.

840 **Figure 6. Complex I inhibition reduces IFN γ receptor activity.** A) PD-L1 transcript was
841 quantified by qRT-PCR using $\Delta\Delta$ Ct relative to β -Actin in macrophages of the indicated genotype
842 after stimulation with 10ng/mL IFN γ . PD-L1 MFI was determined at the same time points by
843 flow cytometry. B) *Ciita* transcript was quantified by qRT-PCR using $\Delta\Delta$ Ct relative to β -Actin
844 *Gapdh* in macrophages of the indicated genotype after stimulation with 10ng/mL IFN γ . MHCII
845 MFI was determined at the same time points by flow cytometry. Data shown are from biological
846 triplicate samples with technical replicates for RT-PCR experiments and are representative of
847 two independent experiments. C) sgNTC (left) or sg*Irf1* (right) macrophages were cultured for
848 24 hours with or without IFN γ stimulation. At 2 hour intervals post-IFN γ stimulation, rotenone
849 was added. After 24 hours of stimulation, cells were harvested and surface expression of MHCII
850 (MFI) was quantified by flow cytometry. Data are mean \pm the standard deviation for 3 biological
851 replicates and are representative of two independent experiments. Statistical testing was
852 performed by one-way ANOVA with Tukey correction for multiple hypothesis testing. D)
853 Control (NTC) or sg*Ndufa1* macrophages were stimulated with IFN γ for the indicated times, and
854 cell lysates analyzed by immunoblot for STAT1 abundance and phosphorylation (Y701 and
855 S727), JAK2 abundance and phosphorylation (Y1007/8), and IFNGR1. Beta-Actin was used as a
856 loading control. Data are representative of three independent experiments. Results shown are
857 from a single experiment analyzed on three parallel blots. p values of 0.05, 0.01, 0.001, and
858 0.001 are indicated by *, **, ***, and ****.

859

860 **Figure 7. Mitochondrial respiration in antigen presenting cells is required IFN γ -dependent**
861 **T cell activation.** A) Cell surface expression of MHCII (MFI) in macrophages (MF) or dendritic
862 cells (DC) derived from conditionally immortalized progenitor lines. IFN γ was added for 24

863 hours where indicated. Cells were treated with vehicle (DMSO), rotenone (10uM), oligomycin
864 (OM, 2.5uM), or CCCP concurrent with IFN γ . Data are three biological replicates and are
865 representative of at least two independent experiments. B) Contour plot of macrophage (top row)
866 or dendritic cell (bottom row) MHCII expression in the absence of (left column) or following
867 (right column) stimulation with IFN γ for 24 hours. Representative samples were selected from
868 (A). The percent MHCII positive are indicated for each of the conditions. C) CD4⁺ T cell
869 activation as measured by the percent of live cells positive for IFN γ by intracellular cytokine
870 staining. Prior to co-culture with T cells, APCs were stimulated with the indicated combinations
871 of IFN γ (10ng/mL), and/or rotenone (10uM) for 24 hours. After washing and pulsing with
872 ESAT-61-15 at the indicated concentrations (nm.), T cells were added to APCs at an effector to
873 target (E:T) ratio of 1:1, and co-cultured for a total of 5 hours. Data are representative of two
874 independent experiments. Data are mean \pm the standard deviation for 3 biological replicates.
875 Statistical testing was performed by one-way ANOVA with Tukey correction for multiple
876 hypothesis testing. D and E) sg*Ndufa1* or NTC macrophages were differentiated from
877 immortalized progenitors, and mixed at the ratios indicated (labeled as percent of KO cells).
878 Mixed cultures were stimulated with IFN γ for 24 hours, peptide loaded, and co-cultured with
879 CD4⁺ T cells (E:T 1:1). Production of IFN γ was measured by ICS and quantified as the percent
880 of cells positive for staining by flow cytometry. Representative contour plots (D) and
881 quantification (E) of the experiment are shown. Data shown are for biological triplicate samples
882 and are representative of two independent experiments. p values of 0.05, 0.01, 0.001, and
883 0.001 are indicated by *, **, ***, and ****.

884

885

886 **Supplementary Figure Legends:**

887 **Figure S1, Related to Figure 3.** A) *sgNTC*, *sgNdufa1*, *sgNdufa2* cells cultured in complete
888 media and treated with or without oligomycin (2.5 μ M) for 4 hours. Relative ATP levels were
889 determined as in Figure 2A B) Intracellular ATP levels quantified as relative light units (RLU)
890 using CellTiterGlo2.0 (Promega) for macrophages in specified growth conditions for 4 hours.
891 Concentrations of carbon source and inhibitors are indicated in Materials and Methods. C)
892 Macrophages were cultured in either glucose or galactose and stimulated with IFN γ for 24 hours.
893 Following stimulation, the proportion of cells with MHCII expression was determined by flow
894 cytometry. D) Macrophages were cultured in conditions as described in Figure 4H. For each
895 condition, cells were stimulated with IFN γ or IFN γ and N-acetylcysteine (NAC) for 24 hours
896 after which cell surface levels of MHCII were quantified. E) Control or complex I mutant
897 (*sgNdufa2*) macrophages were stimulated with IFN γ for 24 hours with increasing doses of
898 mitochondrial reactive oxygen species scavenger MitoTempo. For each concentration, values are
899 plotted as a fold change relative to no scavenger; Mean \pm the standard deviation for 2 biological
900 replicates of each condition. F) Control or complex I deficient macrophages were stimulated
901 with IFN γ for 24 hours with or without the addition of DMOG or 1400W. Following stimulation,
902 the proportion of cells with MHCII expression was determined by flow cytometry. G) Nitric
903 oxide was measured using Griess Reagent System (Promega) from cell supernatants following
904 stimulation with IFN γ and Pam3CSK4 for 24 hours with or without the addition of DMOG or
905 1400W. Relative nitric oxide levels were calculated as a percent relative to control (IFN γ and
906 Pam3CSK4 with DMSO). All data are representative of at least two independent experiments.

907 Statistical testing was performed using one-way ANOVA with Holm-Sidak multiple comparison
908 correction. p values of 0.05, 0.01, 0.001, and 0.001 are indicated by *, **, ***, and ****.

909

910

911 **Figure S2, Related to Figure 7.** A-C) Myeloid progenitors cells were conditionally
912 immortalized by transducing murine bone marrow with an estrogen-dependent Hoxb8 transgene
913 which maintains stem-like properties. Following differentiation of progenitors into macrophages
914 using M-CSF enriched conditioned media, macrophages were stimulated with IFN γ with or
915 without rotenone. 24 hours after stimulation, cell surface levels of (A) MHCII, (B) CD40, (C)
916 and PD-L1 were quantified by flow cytometry. Data are representative of 3 independent
917 experiments and are the mean \pm the standard deviation for 2 biological replicates. Statistical
918 testing was performed by one-way ANOVA with Tukey correction for multiple hypothesis
919 testing. D-F) As in panels A-C, macrophages from either immortalized macrophage progenitors
920 or primary bone marrow were stimulated with IFN γ with or without rotenone or oligomycin. 24
921 hours after stimulation, cell surface levels of (D) MHCII, (E) CD40, (F) and PD-L1 were
922 quantified by flow cytometry. G). Wild-type or Δ Ndufa1 macrophages derived from Hoxb8-
923 immortalized bone marrow progenitors were cultured in the specified media and inhibitor
924 condition before total intracellular ATP was quantified by CellTiterGlo2.0. For each genotype,
925 values are relative to “glucose” control. Mean \pm the standard deviation for 2 biological replicates
926 of each condition. p values of 0.05, 0.01, 0.001, and 0.001 are indicated by *, **, ***, and ****.

927

928

929

930

932 **Bibliography**

933

- 934 1. Mechanisms of costimulation, (2009).
935 2. Attanasio J, Wherry EJ. Costimulatory and Coinhibitory Receptor Pathways in Infectious
936 Disease. *Immunity*. 2016;44(5):1052-68. Epub 2016/05/19. doi:
937 10.1016/j.immuni.2016.04.022. PubMed PMID: 27192569; PMCID: PMC4873956.
938 3. Genetic control of MHC class II expression, (2002).
939 4. Buxadé M, Encabo HH, Riera-Borrull M, Quintana-Gallardo L, López-Cotarelo P,
940 Tellechea M, Martínez-Martínez S, Redondo JM, Martín-Caballero J, Flores JM, Bosch E,
941 Rodríguez-Fernández JL, Aramburu J, López-Rodríguez C. Macrophage-specific MHCII
942 expression is regulated by a remote Ciita enhancer controlled by NFAT5. *Journal of*
943 *Experimental Medicine*. 2018. doi: 10.1084/jem.20180314. PubMed PMID: 30327417.
944 5. Herrero C, Marqués L, Lloberas J, Celada A. IFN- γ -dependent transcription of MHC class
945 II IA is impaired in macrophages from aged mice. *Journal of Clinical Investigation*. 2001.
946 doi: 10.1172/JCI11696. PubMed PMID: 11181648.
947 6. Regulation of MHC class II gene expression by the class II transactivator, (2005).
948 7. Present Yourself! By MHC Class I and MHC Class II Molecules, (2016).
949 8. Steimle V, Siegrist CA, Mottet A, Lisowska-Grospierre B, Mach B. Regulation of MHC
950 class II expression by interferon- γ mediated by the transactivator gene CIITA. *Science*.
951 1994. doi: 10.1126/science.8016643. PubMed PMID: 8016643.
952 9. Wheelock EF. Interferon-Like Virus-Inhibitor Induced in Human Leukocytes by
953 Phytohemagglutinin. *Science*. 1965;149(3681):310-1. Epub 1965/07/16. doi:
954 10.1126/science.149.3681.310. PubMed PMID: 17838106.
955 10. Tominaga K, Yoshimoto T, Torigoe K, Kurimoto M, Matsui K, Hada T, Okamura H,
956 Nakanishi K. IL-12 synergizes with IL-18 or IL-1 β for IFN- γ production from
957 human T cells. *Int Immunol*. 2000;12(2):151-60. Epub 2000/02/02. doi:
958 10.1093/intimm/12.2.151. PubMed PMID: 10653850.
959 11. O'Shea JJ, Paul WE. Regulation of T(H)1 differentiation--controlling the controllers. *Nat*
960 *Immunol*. 2002;3(6):506-8. Epub 2002/05/29. doi: 10.1038/ni0602-506. PubMed PMID:
961 12032561.
962 12. Schneider BE, Korbel D, Hagens K, Koch M, Raupach B, Enders J, Kaufmann SHE,
963 Mittrücker HW, Schaible UE. A role for IL-18 in protective immunity against
964 *Mycobacterium tuberculosis*. *European Journal of Immunology*. 2010. doi:
965 10.1002/eji.200939583.
966 13. Interleukin-12 and the regulation of innate resistance and adaptive immunity, (2003).
967 14. Johnson-Léger C, Hasbold J, Holman M, Klaus GG. The effects of IFN- γ on CD40-
968 mediated activation of B cells from X-linked immunodeficient or normal mice. *The Journal*
969 *of Immunology*. 1997;159:1150-9.
970 15. Alderson MR, Armitage RJ, Tough TW, Strockbine L, Fanslow WC, Spriggs MK. CD40
971 expression by human monocytes: regulation by cytokines and activation of monocytes by
972 the ligand for CD40. *Journal of Experimental Medicine*. 1993;178(2):669-74. doi:
973 10.1084/jem.178.2.669.
974 16. Yamazaki T, Akiba H, Iwai H, Matsuda H, Aoki M, Tanno Y, Shin T, Tsuchiya H, Pardoll
975 DM, Okumura K, Azuma M, Yagita H. Expression of programmed death 1 ligands by

- 976 murine T cells and APC. *J Immunol.* 2002;169(10):5538-45. Epub 2002/11/08. doi:
977 10.4049/jimmunol.169.10.5538. PubMed PMID: 12421930.
- 978 17. Cross-regulation of Signaling Pathways by Interferon- γ : Implications for Immune
979 Responses and Autoimmune Diseases, (2009).
- 980 18. Krawczyk CM, Holowka T, Sun J, Blagih J, Amiel E, DeBerardinis RJ, Cross JR, Jung E,
981 Thompson CB, Jones RG, Pearce EJ. Toll-like receptor-induced changes in glycolytic
982 metabolism regulate dendritic cell activation. *Blood.* 2010. doi: 10.1182/blood-2009-10-
983 249540. PubMed PMID: 20351312.
- 984 19. Liu P-S, Wang H, Li X, Chao T, Teav T, Christen S, Di Conza G, Cheng W-C, Chou C-H,
985 Vavakova M, Muret C, Debackere K, Mazzone M, Huang H-D, Fendt S-M, Ivanisevic J,
986 Ho P-C. α -ketoglutarate orchestrates macrophage activation through metabolic and
987 epigenetic reprogramming. *nature immunology.* 2017;18. doi: 10.1038/ni.3796.
- 988 20. The role of B7 co-stimulation in activation and differentiation of CD4+ and CD8+ T cells,
989 (1998).
- 990 21. Nau GJ, Richmond JFL, Schlesinger A, Jennings EG, Lander ES, Young RA. Human
991 macrophage activation programs induced by bacterial pathogens. *Proceedings of the*
992 *National Academy of Sciences of the United States of America.* 2002;99:1503-8. doi:
993 10.1073/pnas.022649799. PubMed PMID: 11805289.
- 994 22. Schnare M, Barton GM, Holt AC, Takeda K, Akira S, Medzhitov R. Toll-like receptors
995 control activation of adaptive immune responses. *Nature Immunology.* 2001. doi:
996 10.1038/ni712. PubMed PMID: 11547333.
- 997 23. Francisco LM, Sage PT, Sharpe AH. The PD-1 pathway in tolerance and autoimmunity.
998 *Immunol Rev.* 2010;236:219-42. Epub 2010/07/20. doi: 10.1111/j.1600-
999 065X.2010.00923.x. PubMed PMID: 20636820; PMCID: PMC2919275.
- 1000 24. Dendritic cells giveth and taketh away, (2005).
- 1001 25. Brown JA, Dorfman DM, Ma F-R, Sullivan EL, Munoz O, Wood CR, Greenfield EA,
1002 Freeman GJ. Blockade of Programmed Death-1 Ligands on Dendritic Cells Enhances T
1003 Cell Activation and Cytokine Production. *The Journal of Immunology.* 2003;170:1257-66.
1004 doi: 10.4049/jimmunol.170.3.1257.
- 1005 26. Schildberg FA, Klein SR, Freeman GJ, Sharpe AH. Coinhibitory Pathways in the B7-CD28
1006 Ligand-Receptor Family. *Immunity.* 2016;44(5):955-72. Epub 2016/05/19. doi:
1007 10.1016/j.immuni.2016.05.002. PubMed PMID: 27192563; PMCID: PMC4905708.
- 1008 27. Bousoik E, Montazeri Aliabadi H. "Do We Know Jack" About JAK? A Closer Look at
1009 JAK/STAT Signaling Pathway. *Frontiers in Oncology.* 2018. doi:
1010 10.3389/fonc.2018.00287.
- 1011 28. Garcia-Diaz A, Shin DS, Moreno BH, Saco J, Escuin-Ordinas H, Rodriguez GA, Zaretsky
1012 JM, Sun L, Hugo W, Wang X, Parisi G, Saus CP, Torrejon DY, Graeber TG, Comin-
1013 Anduix B, Hu-Lieskovan S, Damoiseaux R, Lo RS, Ribas A. Interferon Receptor Signaling
1014 Pathways Regulating PD-L1 and PD-L2 Expression. *Cell Reports.* 2017. doi:
1015 10.1016/j.celrep.2017.04.031. PubMed PMID: 28494868.
- 1016 29. Ealick SE, Cook WJ, Vijay-Kumar S, Carson M, Nagabhushan TL, Trotta PP, Bugg CE.
1017 Three-dimensional structure of recombinant human interferon-gamma. *Science.*
1018 1991;252(5006):698-702. Epub 1991/05/03. doi: 10.1126/science.1902591. PubMed
1019 PMID: 1902591.

- 1020 30. Pestka S, Krause CD, Walter MR. Interferons, interferon-like cytokines, and their
1021 receptors. *Immunol Rev.* 2004;202:8-32. Epub 2004/11/18. doi: 10.1111/j.0105-
1022 2896.2004.00204.x. PubMed PMID: 15546383.
- 1023 31. Blouin CM, Lamaze C. Interferon gamma receptor: the beginning of the journey. *Front*
1024 *Immunol.* 2013;4:267. Epub 2013/09/13. doi: 10.3389/fimmu.2013.00267. PubMed PMID:
1025 24027571; PMCID: PMC3760442.
- 1026 32. Lasfar A, Cook JR, Cohen Solal KA, Reuhl K, Kottenko SV, Langer JA, Laskin DL.
1027 Critical role of the endogenous interferon ligand-receptors in type I and type II interferons
1028 response. *Immunology.* 2014;142(3):442-52. Epub 2014/03/07. doi: 10.1111/imm.12273.
1029 PubMed PMID: 24597649; PMCID: PMC4080960.
- 1030 33. Meraz MA, White JM, Sheehan KC, Bach EA, Rodig SJ, Dighe AS, Kaplan DH, Riley JK,
1031 Greenlund AC, Campbell D, Carver-Moore K, DuBois RN, Clark R, Aguet M, Schreiber
1032 RD. Targeted disruption of the Stat1 gene in mice reveals unexpected physiologic
1033 specificity in the JAK-STAT signaling pathway. *Cell.* 1996;84(3):431-42. Epub
1034 1996/02/09. doi: 10.1016/s0092-8674(00)81288-x. PubMed PMID: 8608597.
- 1035 34. Schroder K, Hertzog PJ, Ravasi T, Hume DA. Interferon-gamma: an overview of signals,
1036 mechanisms and functions. *J Leukoc Biol.* 2004;75(2):163-89. Epub 2003/10/04. doi:
1037 10.1189/jlb.0603252. PubMed PMID: 14525967.
- 1038 35. Lehtonen A, Matikainen S, Julkunen I. Interferons up-regulate STAT1, STAT2, and IRF
1039 family transcription factor gene expression in human peripheral blood mononuclear cells
1040 and macrophages. *Journal of immunology (Baltimore, Md : 1950).* 1997. PubMed PMID:
1041 9218597.
- 1042 36. Chen J, Feng Y, Lu L, Wang H, Dai L, Li Y, Zhang P. Interferon- γ -induced PD-L1 surface
1043 expression on human oral squamous carcinoma via PKD2 signal pathway. *Immunobiology.*
1044 2012;217(4):385-93. Epub 2011/12/30. doi: 10.1016/j.imbio.2011.10.016. PubMed PMID:
1045 22204817.
- 1046 37. Walser TC, Ma X, Kundu N, Dorsey R, Goloubeva O, Fulton AM. Immune-mediated
1047 modulation of breast cancer growth and metastasis by the chemokine Mig (CXCL9) in a
1048 murine model. *J Immunother.* 2007;30(5):490-8. Epub 2007/06/26. doi:
1049 10.1097/CJI.0b013e318031b551. PubMed PMID: 17589289.
- 1050 38. Lyford-Pike S, Peng S, Young GD, Taube JM, Westra WH, Akpeng B, Bruno TC,
1051 Richmon JD, Wang H, Bishop JA, Chen L, Drake CG, Topalian SL, Pardoll DM, Pai SI.
1052 Evidence for a role of the PD-1:PD-L1 pathway in immune resistance of HPV-associated
1053 head and neck squamous cell carcinoma. *Cancer Res.* 2013;73(6):1733-41. Epub
1054 2013/01/05. doi: 10.1158/0008-5472.Can-12-2384. PubMed PMID: 23288508; PMCID:
1055 PMC3602406.
- 1056 39. Garrido F, Ruiz-Cabello F, Cabrera T, Pérez-Villar JJ, López-Botet M, Duggan-Keen M,
1057 Stern PL. Implications for immunosurveillance of altered HLA class I phenotypes in
1058 human tumours. *Immunol Today.* 1997;18(2):89-95. Epub 1997/02/01. doi: 10.1016/s0167-
1059 5699(96)10075-x. PubMed PMID: 9057360.
- 1060 40. Beatty GL, Paterson Y. Regulation of tumor growth by IFN-gamma in cancer
1061 immunotherapy. *Immunol Res.* 2001;24(2):201-10. Epub 2001/10/12. doi:
1062 10.1385/ir:24:2:201. PubMed PMID: 11594457.
- 1063 41. Pollard KM, Cauvi DM, Toomey CB, Morris KV, Kono DH. Interferon- γ and systemic
1064 autoimmunity. *Discov Med.* 2013;16(87):123-31. Epub 2013/09/04. PubMed PMID:
1065 23998448; PMCID: PMC3934799.

- 1066 42. Lees JR, Cross AH. A little stress is good: IFN-gamma, demyelination, and multiple
1067 sclerosis. *J Clin Invest*. 2007;117(2):297-9. Epub 2007/02/03. doi: 10.1172/jci31254.
1068 PubMed PMID: 17273549; PMCID: PMC1783822.
- 1069 43. Bustamante J, Boisson-Dupuis S, Abel L, Casanova J-L. Mendelian susceptibility to
1070 mycobacterial disease: genetic, immunological, and clinical features of inborn errors of
1071 IFN- γ immunity. *Seminars in Immunology*. 2014;26(6):454 - 70.
- 1072 44. Newport MJ, Huxley CM, Huston S, Hawrylowicz CM, Oostra BA, Williamson R, Levin
1073 M. A Mutation in the Interferon- γ Receptor Gene and Susceptibility to Mycobacterial
1074 Infection. *New England Journal of Medicine*. 1996;335(26):1941-9. doi:
1075 10.1056/nejm199612263352602. PubMed PMID: 8960473.
- 1076 45. Jouanguy E, Altare F, Lamhamedi S, Revy P, Emile J-F, Newport M, Levin M, Blanche S,
1077 Seboun E, Fischer A, Casanova J-L. Interferon- γ Receptor Deficiency in an Infant with
1078 Fatal Bacille Calmette-Guérin Infection. *New England Journal of Medicine*.
1079 1996;335(26):1956-62. doi: 10.1056/nejm199612263352604. PubMed PMID: 8960475.
- 1080 46. Alcaïs A, Fieschi C, Abel L, Casanova J-L. Tuberculosis in children and adults: two
1081 distinct genetic diseases. *The Journal of experimental medicine*. 2005;202:1617-21. doi:
1082 10.1084/jem.20052302. PubMed PMID: 16365144.
- 1083 47. Bogunovic D, Byun M, Durfee LA, Abhyankar A, Sanal O, Mansouri D, Salem S,
1084 Radovanovic I, Grant AV, Adimi P, Mansouri N, Okada S, Bryant VL, Kong X-F, Kreins
1085 A, Velez MM, Boisson B, Khalilzadeh S, Ozcelik U, Darazam IA, Schoggins JW, Rice
1086 CM, Al-Muhsen S, Behr M, Vogt G, Puel A, Bustamante J, Gros P, Huibregtse JM, Abel
1087 L, Boisson-Dupuis S, Casanova J-L. Mycobacterial Disease and Impaired IFN- γ Immunity
1088 in Humans with Inherited ISG15 Deficiency. *Science*. 2012;337.
- 1089 48. Filipe-Santos O, Bustamante J, Chapgier A, Vogt G, de Beaucoudrey L, Feinberg J,
1090 Jouanguy E, Boisson-Dupuis S, Fieschi C, Picard C, Casanova J-L. Inborn errors of IL-
1091 12/23- and IFN-gamma-mediated immunity: molecular, cellular, and clinical features.
1092 *Seminars in immunology*. 2006;18:347-61. doi: 10.1016/j.smim.2006.07.010. PubMed
1093 PMID: 16997570.
- 1094 49. Kong XF, Vogt G, Itan Y, Macura-Biegun A, Szaflarska A, Kowalczyk D, Chapgier A,
1095 Abhyankar A, Furthner D, Djambas Khayat C, Okada S, Bryant VL, Bogunovic D, Kreins
1096 A, Moncada-Vélez M, Migaud M, Al-Ajaji S, Al-Muhsen S, Holland SM, Abel L, Picard
1097 C, Chaussabel D, Bustamante J, Casanova JL, Boisson-Dupuis S. Haploinsufficiency at the
1098 human IFNGR2 locus contributes to mycobacterial disease. *Human Molecular Genetics*.
1099 2013. doi: 10.1093/hmg/dds484.
- 1100 50. Sharpe AH. Introduction to checkpoint inhibitors and cancer immunotherapy. *Immunol*
1101 *Rev*. 2017;276(1):5-8. Epub 2017/03/05. doi: 10.1111/imr.12531. PubMed PMID:
1102 28258698; PMCID: PMC5362112.
- 1103 51. Castro F, Cardoso AP, Goncalves RM, Serre K, Oliveira MJ. Interferon-Gamma at the
1104 Crossroads of Tumor Immune Surveillance or Evasion. *Front Immunol*. 2018;9:847. Epub
1105 2018/05/22. doi: 10.3389/fimmu.2018.00847. PubMed PMID: 29780381; PMCID:
1106 PMC5945880.
- 1107 52. George S, Miao D, Demetri GD, Adeegbe D, Rodig SJ, Shukla S, Lipschitz M, Amin-
1108 Mansour A, Raut CP, Carter SL, Hammerman P, Freeman GJ, Wu CJ, Ott PA, Wong KK,
1109 Van Allen EM. Loss of PTEN Is Associated with Resistance to Anti-PD-1 Checkpoint
1110 Blockade Therapy in Metastatic Uterine Leiomyosarcoma. *Immunity*. 2017;46:197-204.
1111 doi: 10.1016/j.immuni.2017.02.001. PubMed PMID: 28228279.

- 1112 53. Gong B, Kiyotani K, Sakata S, Nagano S, Kumehara S, Baba S, Besse B, Yanagitani N,
1113 Friboulet L, Nishio M, Takeuchi K, Kawamoto H, Fujita N, Katayama R. Secreted PD-L1
1114 variants mediate resistance to PD-L1 blockade therapy in non-small cell lung cancer.
1115 *Journal of Experimental Medicine*. 2019. doi: 10.1084/jem.20180870.
- 1116 54. IFN γ : signalling, epigenetics and roles in immunity, metabolism, disease and cancer
1117 immunotherapy, (2018).
- 1118 55. Mahoney KM, Shukla SA, Patsoukis N, Chaudhri A, Browne EP, Arazi A, Eisenhaure TM,
1119 Pendergraft WF, Hua P, Pham HC, Bu X, Zhu B, Hacohen N, Fritsch EF, Boussiotis VA,
1120 Wu CJ, Freeman GJ. A secreted PD-L1 splice variant that covalently dimerizes and
1121 mediates immunosuppression. *Cancer Immunology, Immunotherapy*. 2019. doi:
1122 10.1007/s00262-018-2282-1. PubMed PMID: 30564891.
- 1123 56. Guak H, Al Habyan S, Ma EH, Aldossary H, Al-Masri M, Won SY, Ying T, Fixman ED,
1124 Jones RG, McCaffrey LM, Krawczyk CM. Glycolytic metabolism is essential for CCR7
1125 oligomerization and dendritic cell migration. *Nat Commun*. 2018;9(1):2463. Epub
1126 2018/06/27. doi: 10.1038/s41467-018-04804-6. PubMed PMID: 29941886; PMCID:
1127 PMC6018630.
- 1128 57. Balic JJ, Albargy H, Luu K, Kirby FJ, Jayasekara WSN, Mansell F, Garama DJ, Nardo
1129 DD, Baschuk N, Louis C, Humphries F, Fitzgerald K, Latz E, Gough DJ, Mansell A.
1130 metabolic reprogramming and IL-1 β expression. *Nature Communications*. 2020;11:1-11.
1131 doi: 10.1038/s41467-020-17669-5.
- 1132 58. Carneiro FRG, Lepelley A, Seeley JJ, Hayden MS, Ghosh S. An Essential Role for ECSIT
1133 in Mitochondrial Complex I Assembly and Mitophagy in Macrophages. *Cell Rep*.
1134 2018;22(10):2654-66. Epub 2018/03/08. doi: 10.1016/j.celrep.2018.02.051. PubMed
1135 PMID: 29514094; PMCID: PMC5909989.
- 1136 59. Everts B, Amiel E, Huang SCC, Smith AM, Chang CH, Lam WY, Redmann V, Freitas TC,
1137 Blagih J, Van Der Windt GJW, Artyomov MN, Jones RG, Pearce EL, Pearce EJ. TLR-
1138 driven early glycolytic reprogramming via the kinases TBK1- $IKK\epsilon$ supports the anabolic
1139 demands of dendritic cell activation. *Nature Immunology*. 2014;15:323-32. doi:
1140 10.1038/ni.2833. PubMed PMID: 24562310.
- 1141 60. Everts B, Amiel E, van der Windt GJ, Freitas TC, Chott R, Yarasheski KE, Pearce EL,
1142 Pearce EJ. Commitment to glycolysis sustains survival of NO-producing inflammatory
1143 dendritic cells. *Blood*. 2012;120(7):1422-31. Epub 2012/07/13. doi: 10.1182/blood-2012-
1144 03-419747. PubMed PMID: 22786879; PMCID: PMC3423780.
- 1145 61. Jha AK, Huang SC, Sergushichev A, Lampropoulou V, Ivanova Y, Loginicheva E,
1146 Chmielewski K, Stewart KM, Ashall J, Everts B, Pearce EJ, Driggers EM, Artyomov MN.
1147 Network integration of parallel metabolic and transcriptional data reveals metabolic
1148 modules that regulate macrophage polarization. *Immunity*. 2015;42(3):419-30. Epub
1149 2015/03/19. doi: 10.1016/j.immuni.2015.02.005. PubMed PMID: 25786174.
- 1150 62. Liu PS, Wang H, Li X, Chao T, Teav T, Christen S, Di Conza G, Cheng WC, Chou CH,
1151 Vavakova M, Muret C, Debackere K, Mazzone M, Huang HD, Fendt SM, Ivanisevic J, Ho
1152 PC. alpha-ketoglutarate orchestrates macrophage activation through metabolic and
1153 epigenetic reprogramming. *Nat Immunol*. 2017;18(9):985-94. Epub 2017/07/18. doi:
1154 10.1038/ni.3796. PubMed PMID: 28714978.
- 1155 63. Mills EL, Kelly B, Logan A, Costa ASH, Varma M, Bryant CE, Tourlomousis P, Dabritz
1156 JHM, Gottlieb E, Latorre I, Corr SC, McManus G, Ryan D, Jacobs HT, Szibor M, Xavier
1157 RJ, Braun T, Frezza C, Murphy MP, O'Neill LA. Succinate Dehydrogenase Supports

- 1158 Metabolic Repurposing of Mitochondria to Drive Inflammatory Macrophages. *Cell*.
1159 2016;167(2):457-70 e13. Epub 2016/09/27. doi: 10.1016/j.cell.2016.08.064. PubMed
1160 PMID: 27667687; PMCID: PMC5863951.
- 1161 64. Jung SB, Choi MJ, Ryu D, Yi HS, Lee SE, Chang JY, Chung HK, Kim YK, Kang SG, Lee
1162 JH, Kim KS, Kim HJ, Kim CS, Lee CH, Williams RW, Kim H, Lee HK, Auwerx J, Shong
1163 M. Reduced oxidative capacity in macrophages results in systemic insulin resistance. *Nat*
1164 *Commun*. 2018;9(1):1551. Epub 2018/04/21. doi: 10.1038/s41467-018-03998-z. PubMed
1165 PMID: 29674655; PMCID: PMC5908799.
- 1166 65. Palmieri EM, Gonzalez-Cotto M, Baseler WA, Davies LC, Ghesquiere B, Maio N, Rice
1167 CM, Rouault TA, Cassel T, Higashi RM, Lane AN, Fan TW, Wink DA, McVicar DW.
1168 Nitric oxide orchestrates metabolic rewiring in M1 macrophages by targeting aconitase 2
1169 and pyruvate dehydrogenase. *Nat Commun*. 2020;11(1):698. Epub 2020/02/06. doi:
1170 10.1038/s41467-020-14433-7. PubMed PMID: 32019928; PMCID: PMC7000728.
- 1171 66. Wang F, Zhang S, Jeon R, Vuckovic I, Jiang X, Lerman A, Folmes CD, Dzeja PD,
1172 Herrmann J. Interferon Gamma Induces Reversible Metabolic Reprogramming of M1
1173 Macrophages to Sustain Cell Viability and Pro-Inflammatory Activity. *EBioMedicine*.
1174 2018. doi: 10.1016/j.ebiom.2018.02.009.
- 1175 67. Baardman J, Verberk SGS, Prange KHM, van Weeghel M, van der Velden S, Ryan DG,
1176 Wust RCI, Neele AE, Speijer D, Denis SW, Witte ME, Houtkooper RH, O'Neill L A,
1177 Knatko EV, Dinkova-Kostova AT, Lutgens E, de Winther MPJ, Van den Bossche J. A
1178 Defective Pentose Phosphate Pathway Reduces Inflammatory Macrophage Responses
1179 during Hypercholesterolemia. *Cell Rep*. 2018;25(8):2044-52 e5. Epub 2018/11/22. doi:
1180 10.1016/j.celrep.2018.10.092. PubMed PMID: 30463003.
- 1181 68. Cheng SC, Quintin J, Cramer RA, Shepardson KM, Saeed S, Kumar V, Giamarellos-
1182 Bourboulis EJ, Martens JHA, Rao NA, Aghajani-refah A, Manjeri GR, Li Y, Ifrim DC, Arts
1183 RJW, Van Der Meer BMJW, Deen PMT, Logie C, O'Neill LA, Willems P, Van De
1184 Veerdonk FL, Van Der Meer JWM, Ng A, Joosten LAB, Wijmenga C, Stunnenberg HG,
1185 Xavier RJ, Netea MG. MTOR- and HIF-1 α -mediated aerobic glycolysis as metabolic basis
1186 for trained immunity. *Science*. 2014. doi: 10.1126/science.1250684. PubMed PMID:
1187 25258083.
- 1188 69. Mills EL, Ryan DG, Prag HA, Dikovskaya D, Menon D, Zaslona Z, Jedrychowski MP,
1189 Costa ASH, Higgins M, Hams E, Szpyt J, Runtsch MC, King MS, McGouran JF, Fischer
1190 R, Kessler BM, McGettrick AF, Hughes MM, Carroll RG, Booty LM, Knatko EV, Meakin
1191 PJ, Ashford MLJ, Modis LK, Brunori G, Sévin DC, Fallon PG, Caldwell ST, Kunji ERS,
1192 Chouchani ET, Frezza C, Dinkova-Kostova AT, Hartley RC, Murphy MP, O'Neill LA.
1193 Itaconate is an anti-inflammatory metabolite that activates Nrf2 via alkylation of KEAP1.
1194 *Nature*. 2018. doi: 10.1038/nature25986. PubMed PMID: 29590092.
- 1195 70. Tannahill GM, Curtis AM, Adamik J, Palsson-Mcdermott EM, McGettrick AF, Goel G,
1196 Frezza C, Bernard NJ, Kelly B, Foley NH, Zheng L, Gardet A, Tong Z, Jany SS, Corr SC,
1197 Haneklaus M, Caffrey BE, Pierce K, Walmsley S, Beasley FC, Cummins E, Nizet V,
1198 Whyte M, Taylor CT, Lin H, Masters SL, Gottlieb E, Kelly VP, Clish C, Auron PE, Xavier
1199 RJ, O'Neill LAJ. Succinate is an inflammatory signal that induces IL-1 β through HIF-1 α .
1200 *Nature*. 2013. doi: 10.1038/nature11986. PubMed PMID: 23535595.
- 1201 71. Veldhoen M, Blankenhaus B, Konjar S, Ferreira C. Metabolic wiring of murine T cell and
1202 intraepithelial lymphocyte maintenance and activation. *Eur J Immunol*. 2018;48(9):1430-
1203 40. Epub 2018/07/26. doi: 10.1002/eji.201646745. PubMed PMID: 30043974.

- 1204 72. Buck MD, O'Sullivan D, Pearce EL. T cell metabolism drives immunity. *J Exp Med*.
1205 2015;212(9):1345-60. Epub 2015/08/12. doi: 10.1084/jem.20151159. PubMed PMID:
1206 26261266; PMCID: PMC4548052.
- 1207 73. Su X, Yu Y, Zhong Y, Giannopoulou EG, Hu X, Liu H, Cross JR, Rättsch G, Rice CM,
1208 Ivashkiv LB. Interferon- γ regulates cellular metabolism and mRNA translation to
1209 potentiate macrophage activation. *Nat Immunol*. 2015;16(8):838-49. Epub 2015/07/07. doi:
1210 10.1038/ni.3205. PubMed PMID: 26147685; PMCID: PMC4509841.
- 1211 74. Doench JG, Fusi N, Sullender M, Hegde M, Vaimberg EW, Donovan KF, Smith I, Tothova
1212 Z, Wilen C, Orchard R, Virgin HW, Listgarten J, Root DE. Optimized sgRNA design to
1213 maximize activity and minimize off-target effects of CRISPR-Cas9. *Nat Biotechnol*.
1214 2016;34(2):184-91. Epub 2016/01/19. doi: 10.1038/nbt.3437. PubMed PMID: 26780180;
1215 PMCID: PMC4744125.
- 1216 75. Li W, Koster J, Xu H, Chen CH, Xiao T, Liu JS, Brown M, Liu XS. Quality control,
1217 modeling, and visualization of CRISPR screens with MAGeCK-VISPR. *Genome Biol*.
1218 2015;16:281. Epub 2015/12/18. doi: 10.1186/s13059-015-0843-6. PubMed PMID:
1219 26673418; PMCID: PMC4699372.
- 1220 76. Ferwerda G, Girardin SE, Kullberg BJ, Le Bourhis L, De Jong DJ, Langenberg DML, Van
1221 Crevel R, Adema GJ, Ottenhoff THM, Van Der Meer JWM, Netea MG. NOD2 and toll-
1222 like receptors are nonredundant recognition systems of Mycobacterium tuberculosis. *PLoS*
1223 *Pathogens*. 2005. doi: 10.1371/journal.ppat.0010034.
- 1224 77. Chapoval AI, Ni J, Lau JS, Wilcox RA, Flies DB, Liu D, Dong H, Sica GL, Zhu G,
1225 Tamada K, Chen L. B7-H3: A costimulatory molecule for T cell activation and IFN- γ
1226 production. *Nature Immunology*. 2001. doi: 10.1038/85339. PubMed PMID: 11224528.
- 1227 78. Steimle V, Durand B, Barras E, Zufferey M, Hadam MR, Mach B, Reith W. A novel DNA-
1228 binding regulatory factor is mutated in primary MHC class II deficiency (bare lymphocyte
1229 syndrome). *Genes and Development*. 1995. doi: 10.1101/gad.9.9.1021. PubMed PMID:
1230 7744245.
- 1231 79. Kiritsy MC, Ankley LM, Trombley JD, Huizinga GP, Lord AE, Orning P, Elling R,
1232 Fitzgerald KA, Olive AJ. A genome-wide screen in macrophages identifies new regulators
1233 of IFN γ -inducible MHCII that contribute to T cell activation. *bioRxiv*. 2020.
- 1234 80. Gu W, Chen J, Yang L, Zhao KN. TNF-alpha promotes IFN-gamma-induced CD40
1235 expression and antigen process in Myb-transformed hematological cells.
1236 *ScientificWorldJournal*. 2012;2012:621969. Epub 2012/05/02. doi: 10.1100/2012/621969.
1237 PubMed PMID: 22547990; PMCID: PMC3322478.
- 1238 81. Kataoka K, Shiraishi Y, Takeda Y, Sakata S, Matsumoto M, Nagano S, Maeda T, Nagata
1239 Y, Kitanaka A, Mizuno S, Tanaka H, Chiba K, Ito S, Watatani Y, Kakiuchi N, Suzuki H,
1240 Yoshizato T, Yoshida K, Sanada M, Itonaga H, Imaizumi Y, Totoki Y, Munakata W,
1241 Nakamura H, Hama N, Shide K, Kubuki Y, Hidaka T, Kameda T, Masuda K, Minato N,
1242 Kashiwase K, Izutsu K, Takaori-Kondo A, Miyazaki Y, Takahashi S, Shibata T,
1243 Kawamoto H, Akatsuka Y, Shimoda K, Takeuchi K, Seya T, Miyano S, Ogawa S. Aberrant
1244 PD-L1 expression through 3'-UTR disruption in multiple cancers. *Nature*. 2016;534:402-6.
1245 doi: 10.1038/nature18294. PubMed PMID: 27281199.
- 1246 82. Burr ML, Sparbier CE, Chan YC, Williamson JC, Woods K, Beavis PA, Lam EYN,
1247 Henderson MA, Bell CC, Stolzenburg S, Gilan O, Bloor S, Noori T, Morgens DW, Bassik
1248 MC, Neeson PJ, Behren A, Darcy PK, Dawson SJ, Voskoboinik I, Trapani JA, Cebon J,

- 1249 Lehner PJ, Dawson MA. CMTM6 maintains the expression of PD-L1 and regulates anti-
1250 Tumour immunity. *Nature*. 2017. doi: 10.1038/nature23643. PubMed PMID: 28813417.
- 1251 83. Coelho MA, de Carné Trécesson S, Rana S, Zecchin D, Moore C, Molina-Arcas M, East P,
1252 Spencer-Dene B, Nye E, Barnouin K, Snijders AP, Lai WS, Blackshear PJ, Downward J.
1253 Oncogenic RAS Signaling Promotes Tumor Immuno-resistance by Stabilizing PD-L1
1254 mRNA. *Immunity*. 2017;47:1083-99.e6. doi: 10.1016/j.immuni.2017.11.016.
- 1255 84. Manguso RT, Pope HW, Zimmer MD, Brown FD, Yates KB, Miller BC, Collins NB, Bi K,
1256 LaFleur MW, Juneja VR, Weiss SA, Lo J, Fisher DE, Miao D, Van Allen E, Root DE,
1257 Sharpe AH, Doench JG, Haining WN. In vivo CRISPR screening identifies Ptpn2 as a
1258 cancer immunotherapy target. *Nature*. 2017;547(7664):413-8. Epub 2017/07/21. doi:
1259 10.1038/nature23270. PubMed PMID: 28723893; PMCID: PMC5924693.
- 1260 85. Mezzadra R, Sun C, Jae LT, Gomez-Eerland R, De Vries E, Wu W, Logtenberg MEW,
1261 Slagter M, Rozeman EA, Hofland I, Broeks A, Horlings HM, Wessels LFA, Blank CU,
1262 Xiao Y, Heck AJR, Borst J, Brummelkamp TR, Schumacher TNM. Identification of
1263 CMTM6 and CMTM4 as PD-L1 protein regulators. *Nature*. 2017. doi:
1264 10.1038/nature23669. PubMed PMID: 28813410.
- 1265 86. Hassounah NB, Malladi VS, Huang Y, Freeman SS, Beauchamp EM, Koyama S, Souders
1266 N, Martin S, Dranoff G, Wong KK, Pedomallu CS, Hammerman PS, Akbay EA.
1267 Identification and characterization of an alternative cancer-derived PD-L1 splice variant.
1268 *Cancer Immunology, Immunotherapy*. 2019. doi: 10.1007/s00262-018-2284-z. PubMed
1269 PMID: 30564890.
- 1270 87. Kriegsman BA, Vangala P, Chen BJ, Meraner P, Brass AL, Garber M, Rock KL. Frequent
1271 Loss of IRF2 in Cancers Leads to Immune Evasion through Decreased MHC Class I
1272 Antigen Presentation and Increased PD-L1 Expression. *The Journal of Immunology*.
1273 2019;203:1999-2010. doi: 10.4049/jimmunol.1900475. PubMed PMID: 31471524.
- 1274 88. Papalexli E, Mimitou E, Butler AW, Foster S, Bracken B, Mauck WM, Wessels H-H,
1275 Yeung BZ, Smibert P, Satija R. Characterizing the molecular regulation of inhibitory
1276 immune checkpoints with multi-modal single-cell screens. *bioRxiv*.
1277 2020:2020.06.28.175596. doi: 10.1101/2020.06.28.175596.
- 1278 89. Wang P, Geng J, Gao J, Zhao H, Li J, Shi Y, Yang B, Xiao C, Linghu Y, Sun X, Chen X,
1279 Hong L, Qin F, Li X, Yu JS, You H, Yuan Z, Zhou D, Johnson RL, Chen L. Macrophage
1280 achieves self-protection against oxidative stress-induced ageing through the Mst-Nrf2 axis.
1281 *Nat Commun*. 2019;10(1):755. Epub 2019/02/16. doi: 10.1038/s41467-019-08680-6.
1282 PubMed PMID: 30765703; PMCID: PMC6376064.
- 1283 90. Wijdeven RH, van Luijn MM, Wierenga-Wolf AF, Akkermans JJ, van den Elsen PJ,
1284 Hintzen RQ, Neefjes J. Chemical and genetic control of IFN γ -induced MHCII
1285 expression. *EMBO Rep*. 2018;19(9). Epub 2018/07/20. doi: 10.15252/embr.201745553.
1286 PubMed PMID: 30021835; PMCID: PMC6123650.
- 1287 91. Liu B, Liao J, Rao X, Kushner SA, Chung CD, Chang DD, Shuai K. Inhibition of Stat1-
1288 mediated gene activation by PIAS1. *Proc Natl Acad Sci U S A*. 1998;95(18):10626-31.
1289 Epub 1998/09/02. doi: 10.1073/pnas.95.18.10626. PubMed PMID: 9724754; PMCID:
1290 PMC27945.
- 1291 92. Subramanian A, Tamayo P, Mootha VK, Mukherjee S, Ebert BL, Gillette MA, Paulovich
1292 A, Pomeroy SL, Golub TR, Lander ES, Mesirov JP. Gene set enrichment analysis: A
1293 knowledge-based approach for interpreting genome-wide expression profiles. *Proceedings*

- 1294 of the National Academy of Sciences of the United States of America. 2005. doi:
1295 10.1073/pnas.0506580102. PubMed PMID: 16199517.
- 1296 93. Stroud DA, Surgenor EE, Formosa LE, Reljic B, Frazier AE, Dibley MG, Osellame LD,
1297 Stait T, Beilharz TH, Thorburn DR, Salim A, Ryan MT. Accessory subunits are integral for
1298 assembly and function of human mitochondrial complex I. *Nature*. 2016;538(7623):123-6.
1299 Epub 2016/09/15. doi: 10.1038/nature19754. PubMed PMID: 27626371.
- 1300 94. Lazarou M, McKenzie M, Ohtake A, Thorburn DR, Ryan MT. Analysis of the Assembly
1301 Profiles for Mitochondrial- and Nuclear-DNA-Encoded Subunits into Complex I.
1302 *Molecular and Cellular Biology*. 2007;27:4228-37.
- 1303 95. Pagliarini DJ, Calvo SE, Chang B, Sheth SA, Vafai SB, Ong SE, Walford GA, Sugiana C,
1304 Boneh A, Chen WK, Hill DE, Vidal M, Evans JG, Thorburn DR, Carr SA, Mootha VK. A
1305 mitochondrial protein compendium elucidates complex I disease biology. *Cell*.
1306 2008;134(1):112-23. Epub 2008/07/11. doi: 10.1016/j.cell.2008.06.016. PubMed PMID:
1307 18614015; PMCID: PMC2778844.
- 1308 96. Baradaran R, Berrisford JM, Minhas GS, Sazanov LA. Crystal structure of the entire
1309 respiratory complex I. *Nature*. 2013;494(7438):443-8. doi: 10.1038/nature11871.
- 1310 97. Zickermann V, Wirth C, Nasiri H, Siegmund K, Schwalbe H, Hunte C, Brandt U.
1311 Mechanistic insight from the crystal structure of mitochondrial complex I. *Science*.
1312 2015;347:44-9.
- 1313 98. Zhu J, Vinothkumar KR, Hirst J. Structure of mammalian respiratory complex I. *Nature*.
1314 2016;536(7616):354-8. doi: 10.1038/nature19095.
- 1315 99. Barrientos A, Moraes CT. Titrating the effects of mitochondrial complex I impairment in
1316 the cell physiology. *J Biol Chem*. 1999;274(23):16188-97. Epub 1999/05/29. doi:
1317 10.1074/jbc.274.23.16188. PubMed PMID: 10347173.
- 1318 100. Brand MD, Nicholls DG. Assessing mitochondrial dysfunction in cells. *Biochem J*.
1319 2011;435(2):297-312. Epub 2011/07/06. doi: 10.1042/BJ20110162. PubMed PMID:
1320 21726199; PMCID: PMC3076726.
- 1321 101. Vacanti Nathaniel M, Divakaruni Ajit S, Green Courtney R, Parker Seth J, Henry Robert R,
1322 Ciaraldi Theodore P, Murphy Anne N, Metallo Christian M. Regulation of Substrate
1323 Utilization by the Mitochondrial Pyruvate Carrier. *Molecular Cell*. 2014;56(3):425-35. doi:
1324 <https://doi.org/10.1016/j.molcel.2014.09.024>.
- 1325 102. De Vriese AS, Van Coster R, Smet J, Seneca S, Lovering A, Van Haute LL,
1326 Vanopdenbosch LJ, Martin JJ, Ceuterick-De Groote C, Vandecasteele S, Boelaert JR.
1327 Linezolid-induced inhibition of mitochondrial protein synthesis. *Clinical Infectious*
1328 *Diseases*. 2006;42:1111-7. doi: 10.1086/501356.
- 1329 103. Soriano A, Miró O, Mensa J. Mitochondrial Toxicity Associated with Linezolid. *New*
1330 *England Journal of Medicine*. 2005;353:2305-6. doi: 10.1056/NEJM200511243532123.
- 1331 104. Wilson DN, Schlutzen F, Harms JM, Starosta AL, Connell SR, Fucini P. The
1332 oxazolidinone antibiotics perturb the ribosomal peptidyl-transferase center and effect tRNA
1333 positioning. *Proc Natl Acad Sci U S A*. 2008;105(36):13339-44. Epub 2008/09/02. doi:
1334 10.1073/pnas.0804276105. PubMed PMID: 18757750; PMCID: PMC2533191.
- 1335 105. Bustamante E, Morris HP, Pedersen PL. Hexokinase: The Direct Link between
1336 Mitochondrial and Glycolytic Reactions in Rapidly Growing Cancer Cells. Springer,
1337 Boston, MA; 1978. p. 363-80.
- 1338 106. Cramer T, Yamanishi Y, Clausen BE, Förster I, Pawlinski R, Mackman N, Haase VH,
1339 Jaenisch R, Corr M, Nizet V, Firestein GS, Gerber HP, Ferrara N, Johnson RS. HIF-1 α is

- 1340 essential for myeloid cell-mediated inflammation. *Cell*. 2003;112:645-57. doi:
1341 10.1016/S0092-8674(03)00154-5. PubMed PMID: 12628185.
- 1342 107. Hypoxia-inducible factors in physiology and medicine, (2012).
- 1343 108. Braverman J, Stanley SA. Nitric Oxide Modulates Macrophage Responses to
1344 Mycobacterium tuberculosis Infection through Activation of HIF-1 α and Repression of NF-
1345 κ B The *Journal of Immunology*. 2017. doi: 10.4049/jimmunol.1700515.
- 1346 109. Mishra BB, Rathinam VAK, Martens GW, Martinot AJ, Kornfeld H, Fitzgerald KA,
1347 Sassetti CM. Nitric oxide controls the immunopathology of tuberculosis by inhibiting
1348 NLRP3 inflammasome-dependent processing of IL-1 β . *Nature Immunology*. 2013. doi:
1349 10.1038/ni.2474.
- 1350 110. Wang GG, Calvo KR, Pasillas MP, Sykes DB, Häcker H, Kamps MP. Quantitative
1351 production of macrophages or neutrophils ex vivo using conditional Hoxb8. *Nature*
1352 *Methods*. 2006. doi: 10.1038/nmeth865.
- 1353 111. Redecke V, Wu R, Zhou J, Finkelstein D, Chaturvedi V, High AA, Häcker H.
1354 Hematopoietic progenitor cell lines with myeloid and lymphoid potential. *Nature Methods*.
1355 2013. doi: 10.1038/nmeth.2510.
- 1356 112. Gallegos AM, Pamer EG, Glickman MS. Delayed protection by ESAT-6-specific effector
1357 CD4⁺ T cells after airborne M. tuberculosis infection. *Journal of Experimental Medicine*.
1358 2008. doi: 10.1084/jem.20080353. PubMed PMID: 18779346.
- 1359 113. Bhat MY, Solanki HS, Advani J, Khan AA, Keshava Prasad TS, Gowda H, Thiyagarajan S,
1360 Chatterjee A. Comprehensive network map of interferon gamma signaling. *J Cell Commun*
1361 *Signal*. 2018;12(4):745-51. Epub 2018/09/08. doi: 10.1007/s12079-018-0486-y. PubMed
1362 PMID: 30191398; PMCID: PMC6235777.
- 1363 114. Cameron AM, Castoldi A, Sanin DE, Flachsmann LJ, Field CS, Puleston DJ, Kyle RL,
1364 Patterson AE, Hässler F, Buescher JM, Kelly B, Pearce EL, Pearce EJ. Inflammatory
1365 macrophage dependence on NAD⁺ salvage is a consequence of reactive oxygen species-
1366 mediated DNA damage. *Nature Immunology*. 2019. doi: 10.1038/s41590-019-0336-y.
- 1367 115. Venter G, Oerlemans FTJJ, Willemsse M, Wijers M, Franssen JAM, Wieringa B. NAMPT-
1368 Mediated Salvage Synthesis of NAD⁺ Controls Morphofunctional Changes of
1369 Macrophages. *PLoS ONE*. 2014;9:e97378. doi: 10.1371/journal.pone.0097378.
- 1370 116. Minhas PS, Liu L, Moon PK, Joshi AU, Dove C, Mhatre S, Contrepois K, Wang Q, Lee
1371 BA, Coronado M, Bernstein D, Snyder MP, Migaud M, Majeti R, Mochly-Rosen D,
1372 Rabinowitz JD, Andreasson KI. Macrophage de novo NAD(+) synthesis specifies immune
1373 function in aging and inflammation. *Nat Immunol*. 2019;20(1):50-63. Epub 2018/11/28.
1374 doi: 10.1038/s41590-018-0255-3. PubMed PMID: 30478397; PMCID: PMC6768398.
- 1375 117. Lv H, Lv G, Chen C, Zong Q, Jiang G, Ye D, Cui X, He Y, Xiang W, Han Q, Tang L,
1376 Yang W, Wang H. NAD(+) Metabolism Maintains Inducible PD-L1 Expression to Drive
1377 Tumor Immune Evasion. *Cell Metab*. 2020. Epub 2020/11/11. doi:
1378 10.1016/j.cmet.2020.10.021. PubMed PMID: 33171124.
- 1379 118. Heng TS, Painter MW. The Immunological Genome Project: networks of gene expression
1380 in immune cells. *Nat Immunol*. 2008;9(10):1091-4. Epub 2008/09/19. doi: 10.1038/ni1008-
1381 1091. PubMed PMID: 18800157.
- 1382 119. Lipid and small-molecule display by CD1 and MR1, (2015).
- 1383 120. Benson SA, Ernst JD. TLR2-dependent inhibition of macrophage responses to IFN- γ is
1384 mediated by distinct, gene-specific mechanisms. *PLoS ONE*. 2009. doi:
1385 10.1371/journal.pone.0006329. PubMed PMID: 19629181.

- 1386 121. Fortune SM, Solache A, Jaeger A, Hill PJ, Belisle JT, Bloom BR, Rubin EJ, Ernst JD.
1387 Mycobacterium tuberculosis Inhibits Macrophage Responses to IFN- γ through Myeloid
1388 Differentiation Factor 88-Dependent and -Independent Mechanisms The Journal of
1389 Immunology. 2004. doi: 10.4049/jimmunol.172.10.6272. PubMed PMID: 15128816.
- 1390 122. Kincaid EZ, Wolf AJ, Desvignes L, Mahapatra S, Crick DC, Brennan PJ, Pavelka MS, Jr.,
1391 Ernst JD. Codominance of TLR2-dependent and TLR2-independent modulation of MHC
1392 class II in Mycobacterium tuberculosis infection in vivo. J Immunol. 2007;179(5):3187-95.
1393 Epub 2007/08/22. doi: 10.4049/jimmunol.179.5.3187. PubMed PMID: 17709534.
- 1394 123. Su YM, Teemu P.; Mu, Luye; Mirek, Emily; Manalis, Scott R.; Anthony, Tracy G.; Sesaki,
1395 Hiromi; Chen, Jianzhu. Disassembly of ETC Complexes Drives Macrophage Inflammatory
1396 Responses by Reprogramming Cellular Metabolism and Translation. Available at SSRN:
1397 <https://ssrncom/abstract=3611881> or <http://dxdoiorg/102139/ssrn3611881>. 2020.
- 1398 124. Jang S, Javadov S. OPA1 regulates respiratory supercomplexes assembly: The role of
1399 mitochondrial swelling. Mitochondrion. 2020. doi: 10.1016/j.mito.2019.11.006. PubMed
1400 PMID: 31870826.
- 1401 125. Blasi E, Radzioch D, Merletti L, Varesio L. Generation of macrophage cell line from fresh
1402 bone marrow cells with a myc/raf recombinant retrovirus. Cancer biochemistry biophysics.
1403 1989. PubMed PMID: 2695237.
- 1404 126. Joung J, Konermann S, Gootenberg JS, Abudayyeh OO, Platt RJ, Brigham MD, Sanjana
1405 NE, Zhang F. Genome-scale CRISPR-Cas9 knockout and transcriptional activation
1406 screening. Nature Protocols. 2017. doi: 10.1038/nprot.2017.016. PubMed PMID:
1407 28333914.
- 1408 127. Brown MB. 400: A Method for Combining Non-Independent, One-Sided Tests of
1409 Significance. Biometrics. 1975;31(4):987-92. doi: 10.2307/2529826.
- 1410 128. Jia G, Wang X, Xiao G. A permutation-based non-parametric analysis of CRISPR screen
1411 data. BMC Genomics. 2017;18(1):545. Epub 2017/07/21. doi: 10.1186/s12864-017-3938-
1412 5. PubMed PMID: 28724352; PMCID: PMC5518132.
- 1413 129. Bodapati S, Daley TP, Lin X, Zou J, Qi LS. A benchmark of algorithms for the analysis of
1414 pooled CRISPR screens. Genome Biology. 2020;21(1):62. doi: 10.1186/s13059-020-
1415 01972-x.
- 1416 130. Merico D, Isserlin R, Stueker O, Emili A, Bader GD. Enrichment map: A network-based
1417 method for gene-set enrichment visualization and interpretation. PLoS ONE. 2010. doi:
1418 10.1371/journal.pone.0013984. PubMed PMID: 21085593.
- 1419 131. Reimand J, Isserlin R, Voisin V, Kucera M, Tannus-Lopes C, Rostamianfar A, Wadi L,
1420 Meyer M, Wong J, Xu C, Merico D, Bader GD. Pathway enrichment analysis and
1421 visualization of omics data using g:Profiler, GSEA, Cytoscape and EnrichmentMap. Nature
1422 Protocols. 2019. doi: 10.1038/s41596-018-0103-9. PubMed PMID: 30664679.
- 1423 132. Fulco CP, Munschauer M, Anyoha R, Munson G, Grossman SR, Perez EM, Kane M,
1424 Cleary B, Lander ES, Engreitz JM. Systematic mapping of functional enhancer-promoter
1425 connections with CRISPR interference. Science. 2016. doi: 10.1126/science.aag2445.
- 1426 133. Field CS, Baixauli F, Kyle RL, Puleston DJ, Cameron AM, Sanin DE, Hippen KL, Loschi
1427 M, Thangavelu G, Corrado M, Edwards-Hicks J, Grzes KM, Pearce EJ, Blazar BR, Pearce
1428 EL. Mitochondrial Integrity Regulated by Lipid Metabolism Is a Cell-Intrinsic Checkpoint
1429 for Treg Suppressive Function. Cell Metabolism. 2020. doi: 10.1016/j.cmet.2019.11.021.
1430 PubMed PMID: 31883840.

- 1431 134. Horlbeck MA, Xu A, Wang M, Bennett NK, Park CY, Bogdanoff D, Adamson B, Chow
1432 ED, Kampmann M, Peterson TR, Nakamura K, Fischbach MA, Weissman JS, Gilbert LA.
1433 Mapping the Genetic Landscape of Human Cells. *Cell*. 2018. doi:
1434 10.1016/j.cell.2018.06.010. PubMed PMID: 30033366.
1435

Figure 1

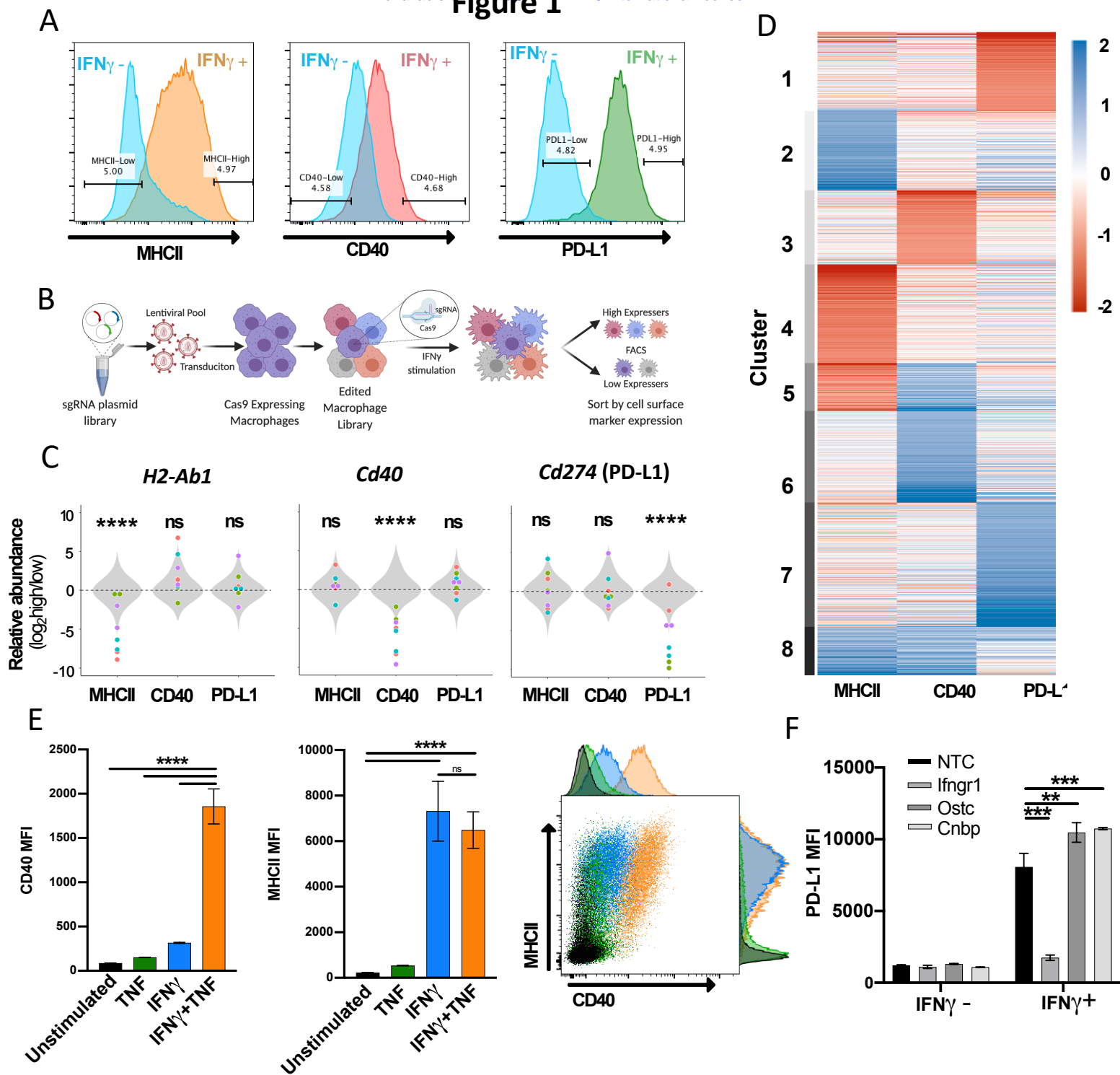


Figure 2

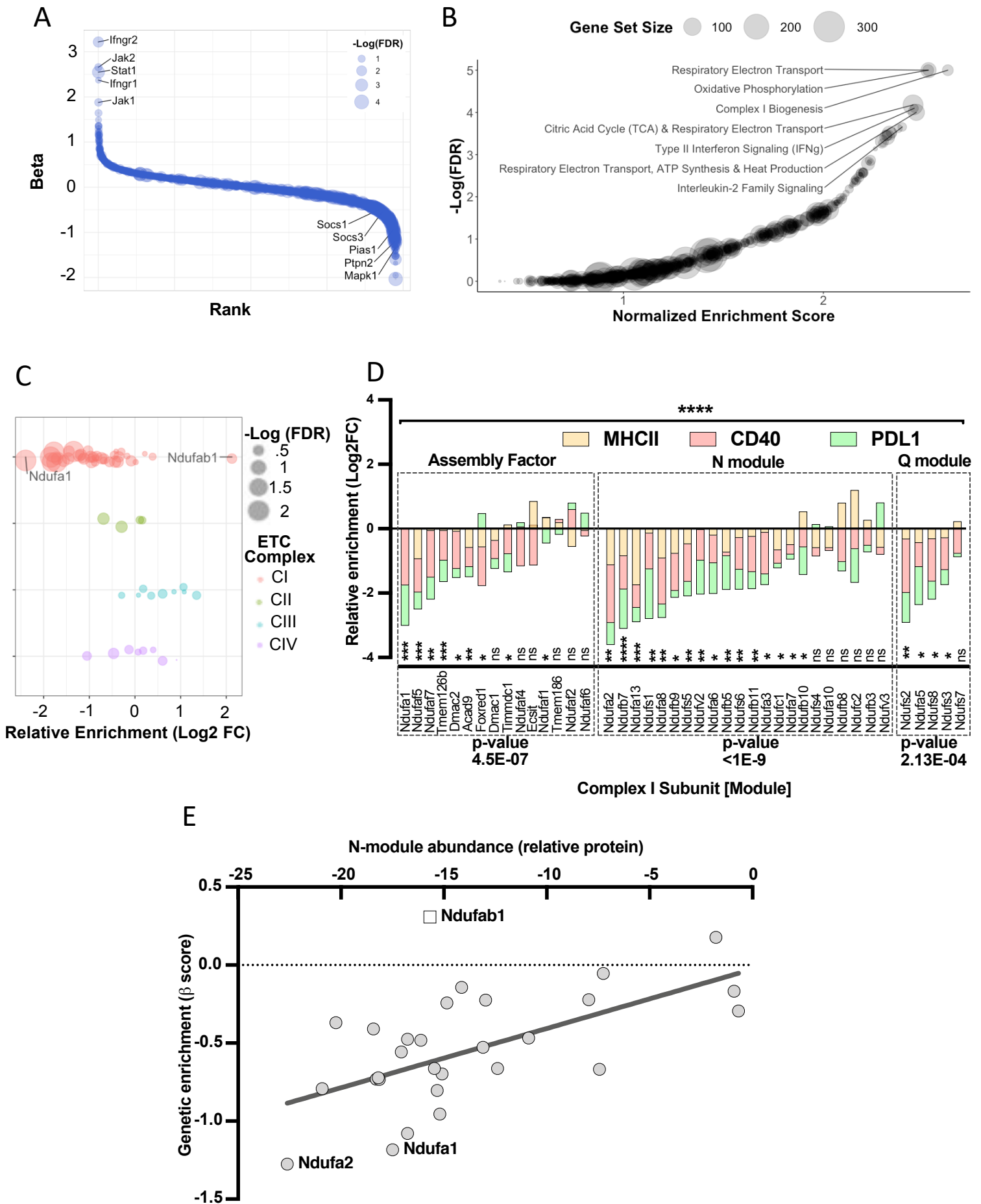


Figure 3

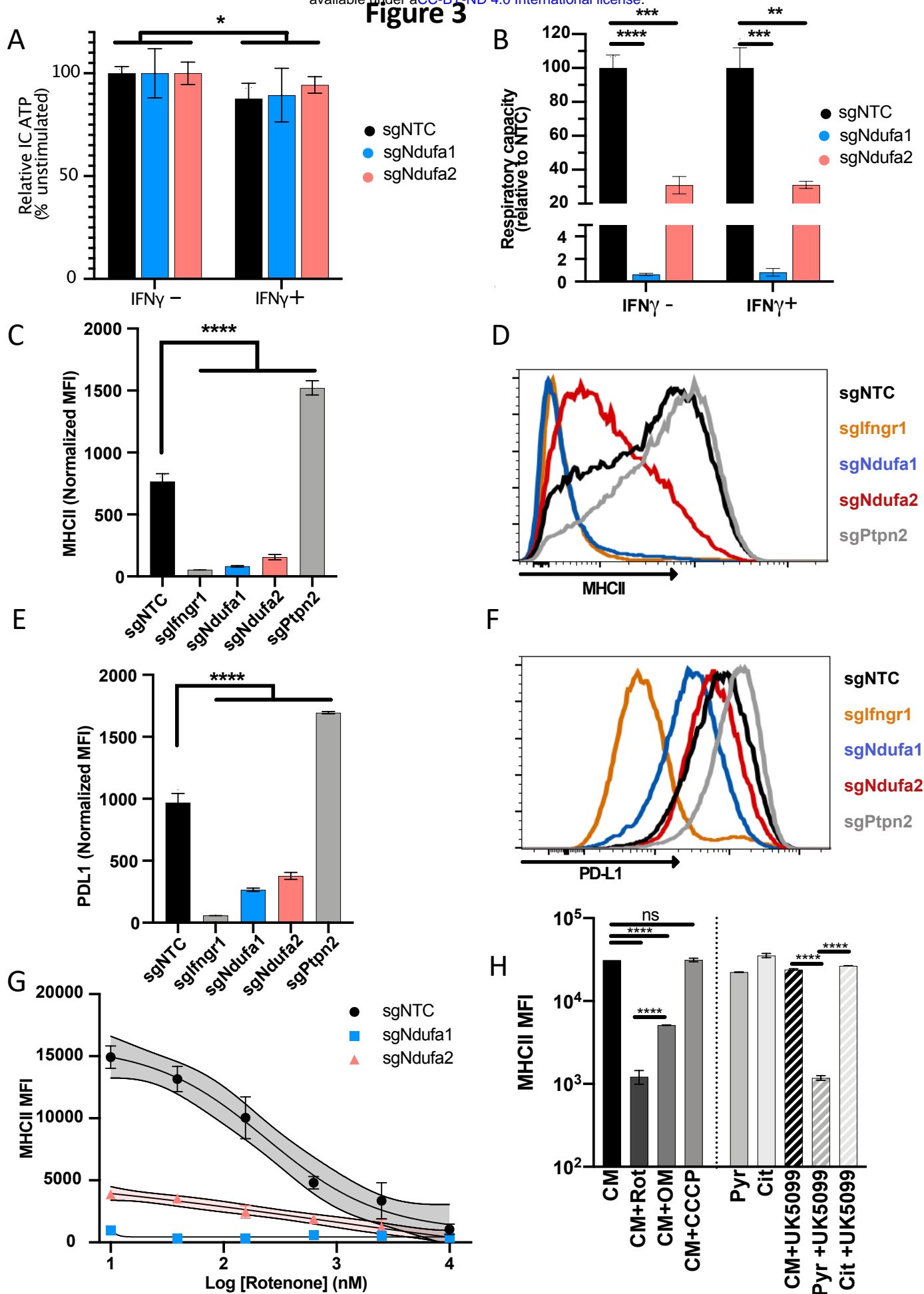
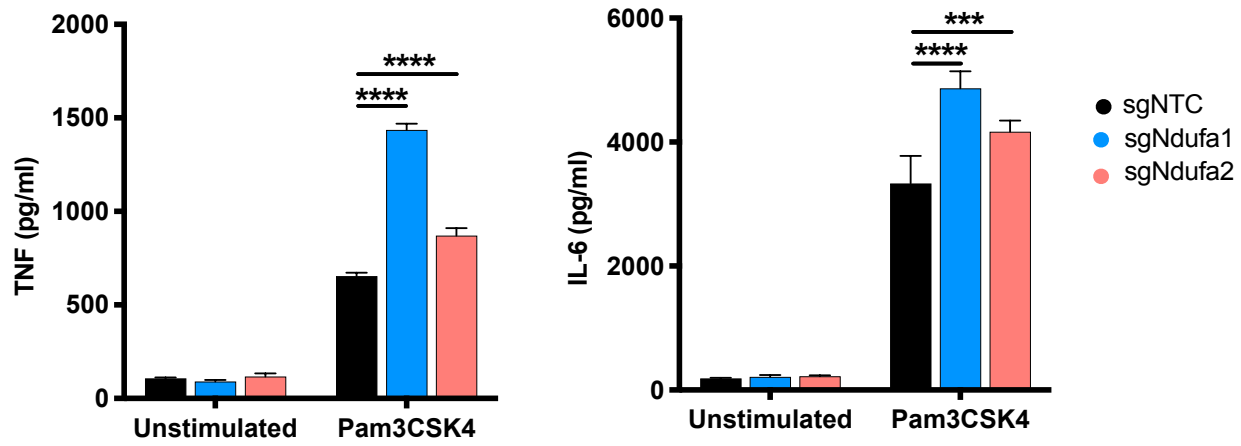
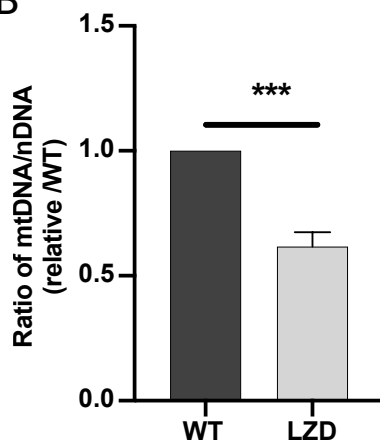


Figure 4

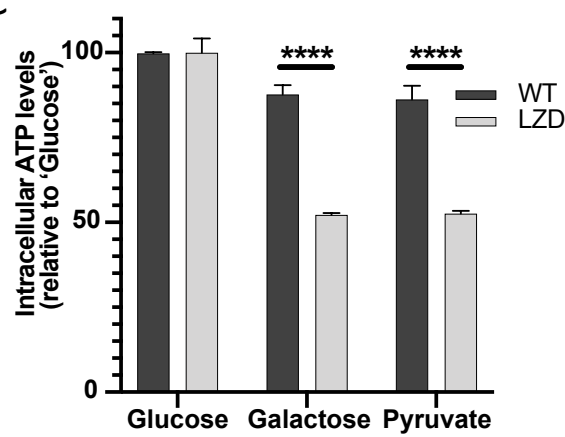
A



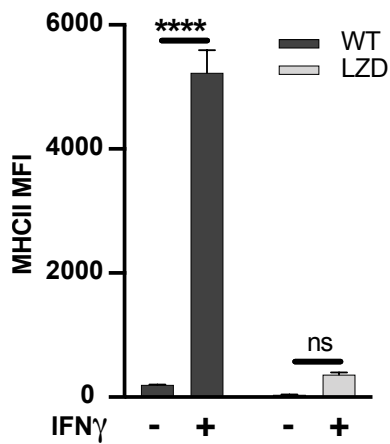
B



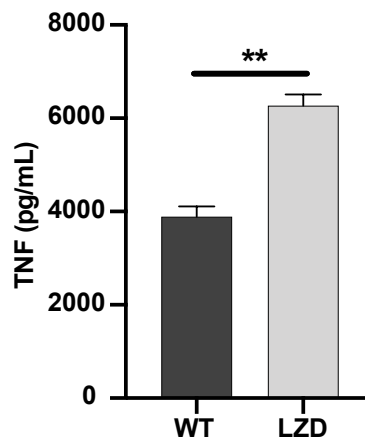
C



D



E



F

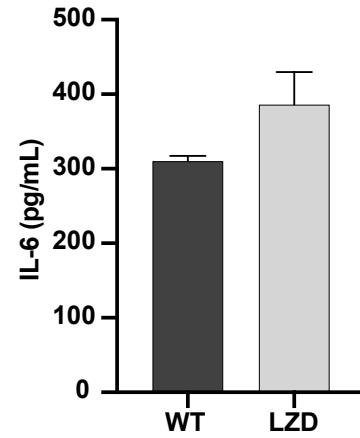


Figure 5

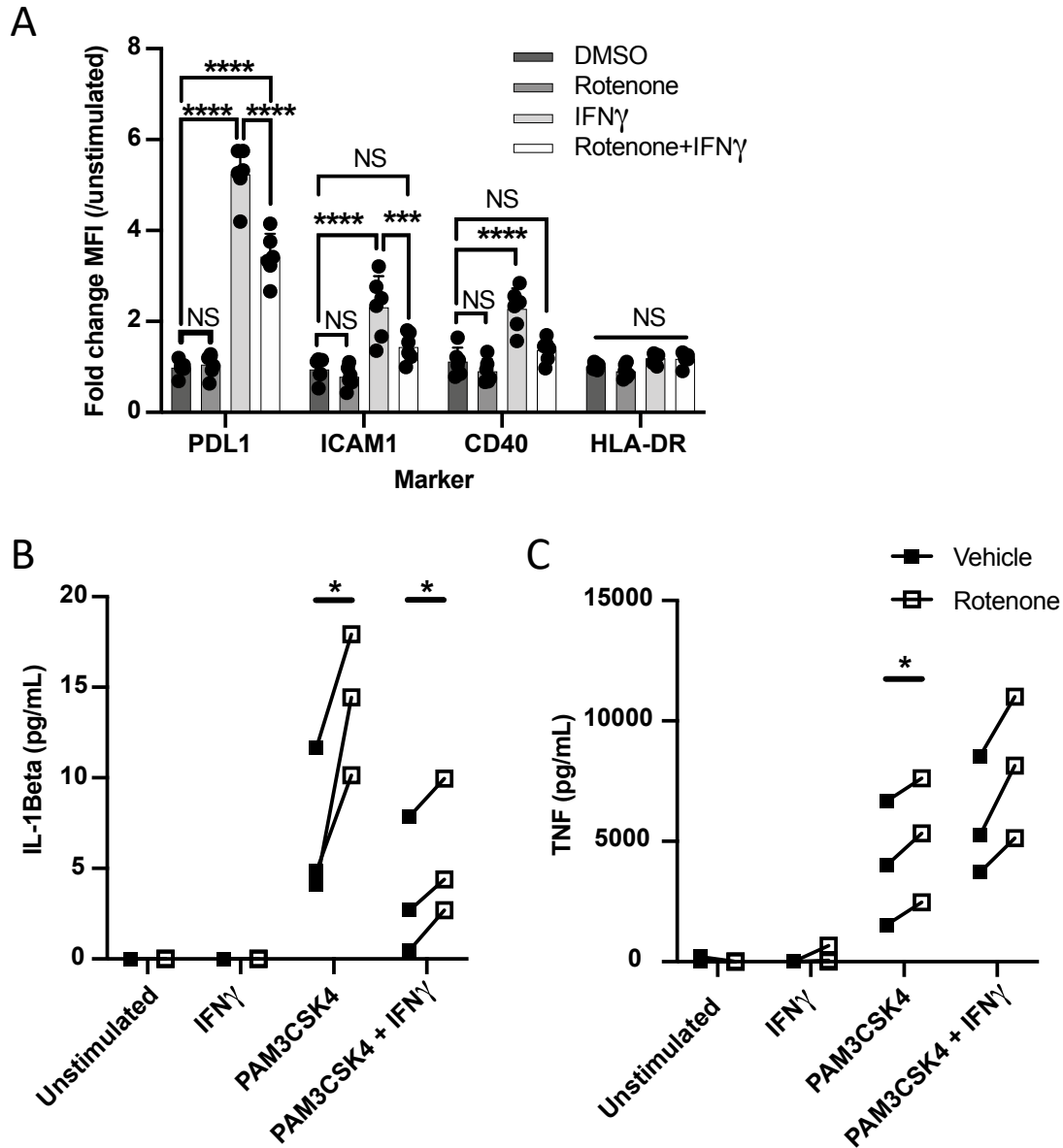


Figure 6

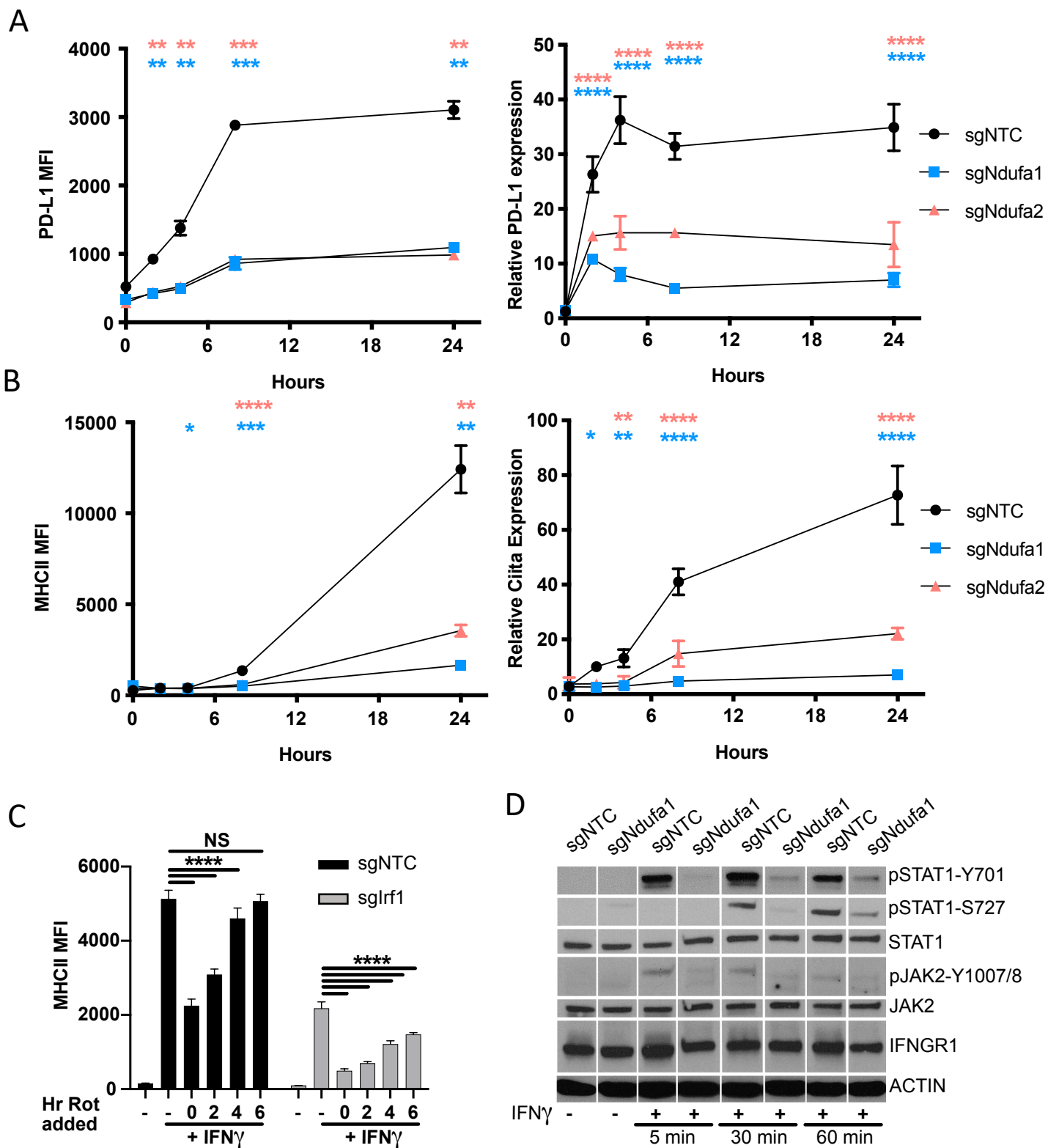
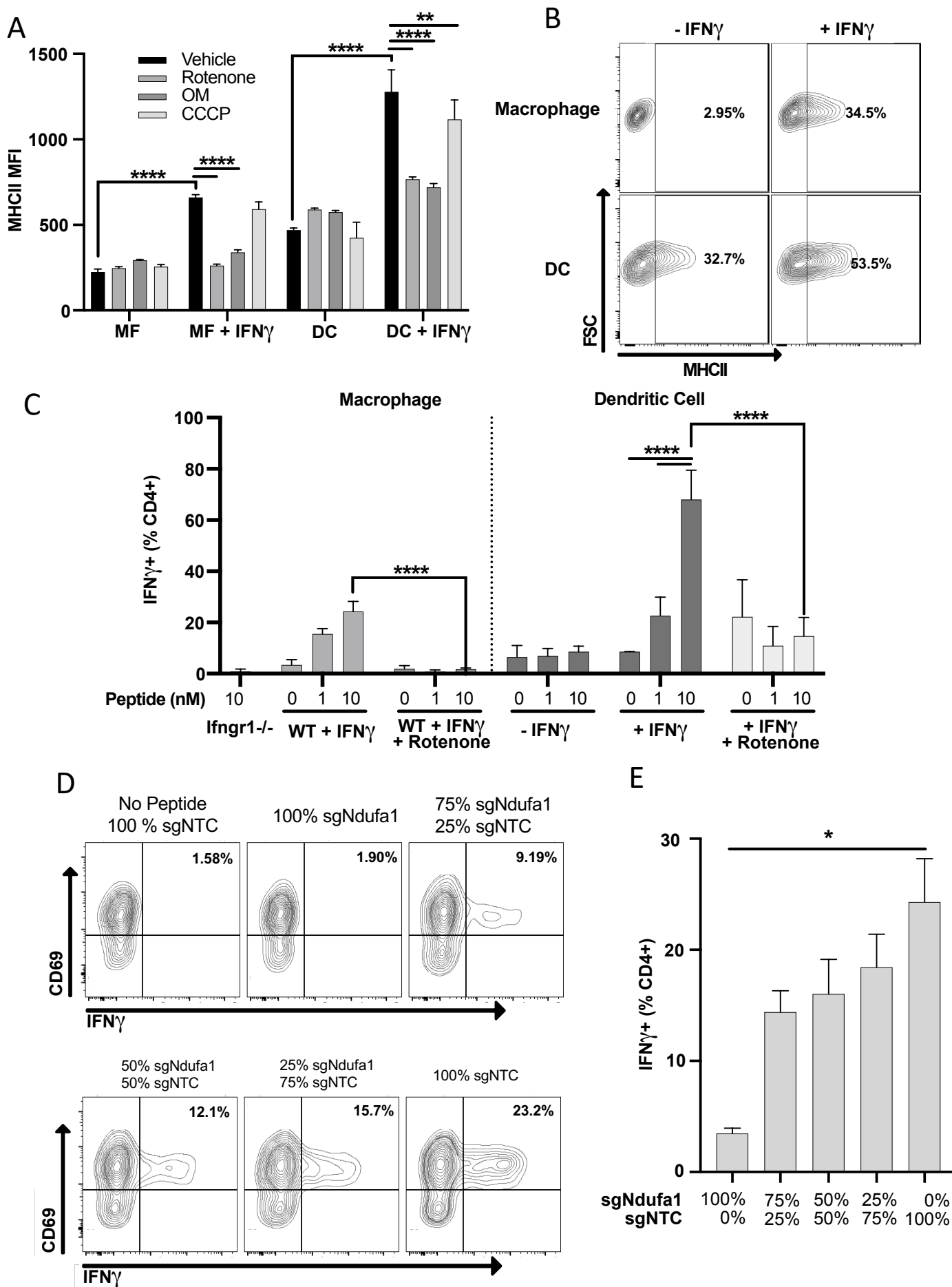
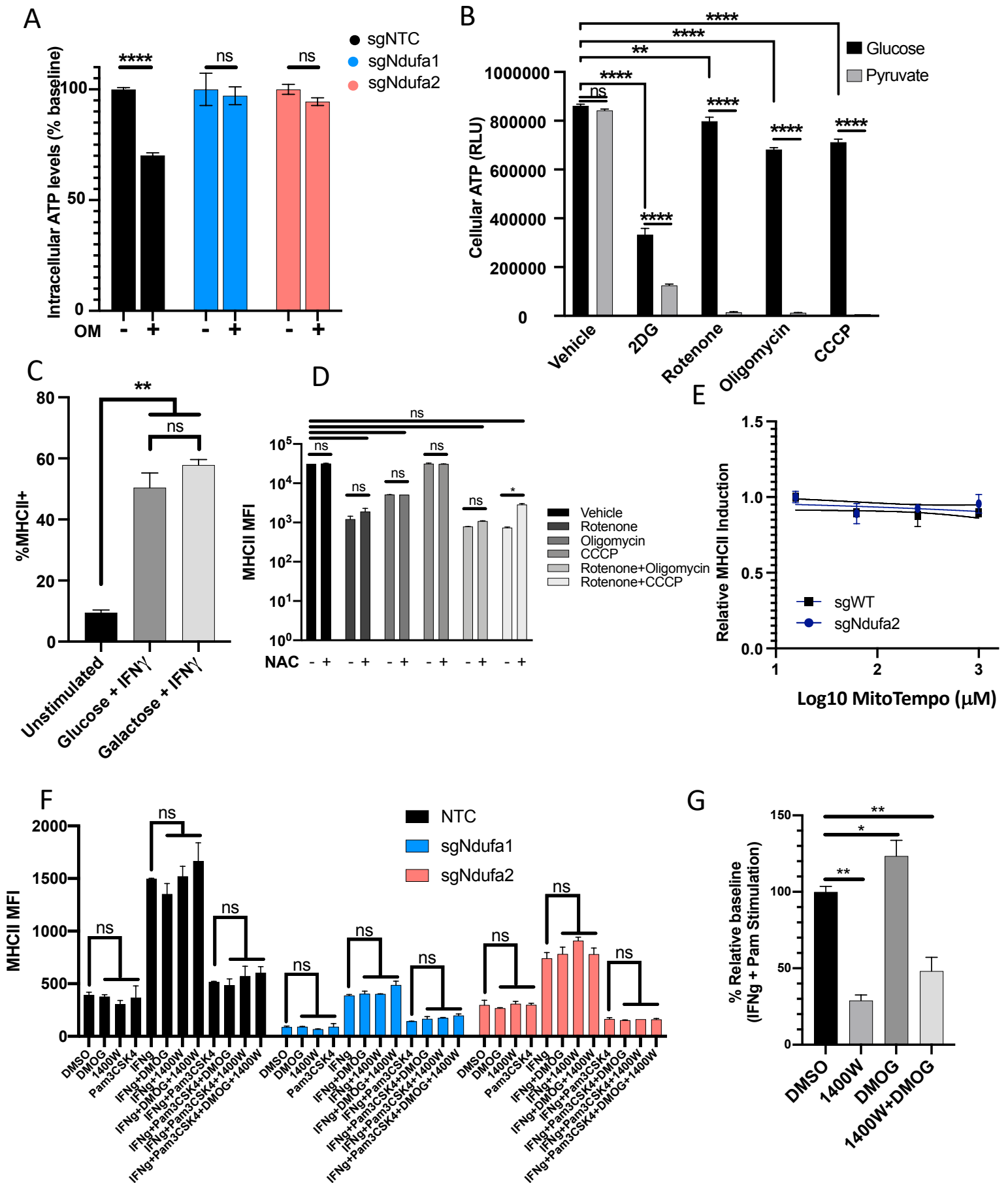


Figure 7



Supplemental Figure 1



Supplemental Figure 2

